Available online at www.sciencedirect.com
ScienceDirect
Journal of Computational Physics 227 (2008) 2514–2539
JOURNAL OF COMPUTATIONAL PHYSICS
www.elsevier.com/locate/jcp

# A quadrature-based moment method for dilute fluid-particle flows

O. Desjardins [a], R.O. Fox [b,*], P. Villedieu [c]

[a] Center for Turbulence Research, Building 500, Stanford University, Stanford, CA 94000, USA
[b] Department of Chemical and Biological Engineering, 2114 Sweeney Hall, Iowa State University, Ames, IA 50011-2230, USA
[c] ONERA, 2 Avenue Edmond-Belin, 31077 Toulouse, France

Received 9 March 2007; received in revised form 25 October 2007; accepted 31 October 2007
Available online 17 November 2007

**Abstract**

Gas-particle and other dispersed-phase flows can be described by a kinetic equation containing terms for spatial transport, acceleration, and particle processes (such as evaporation or collisions). In principle, the kinetic description is valid from the dilute (non-collisional) to the dense limit. However, its numerical solution in multi-dimensional systems is intractable due to the large number of independent variables. As an alternative, Lagrangian methods "discretize" the density function into "parcels" that are simulated using Monte-Carlo methods. While quite accurate, as in any statistical approach, Lagrangian methods require a relatively large number of parcels to control statistical noise, and thus are computationally expensive. A less costly alternative is to solve Eulerian transport equations for selected moments of the kinetic equation. However, it is well known that in the dilute limit Eulerian methods have great difficulty to describe correctly the moments as predicted by a Lagrangian method. Here a two-node quadrature-based Eulerian moment closure is developed and tested for the kinetic equation. It is shown that the method can successfully handle highly non-equilibrium flows (e.g. impinging particle jets, jet crossing, particle rebound off walls, finite Stokes number flows) that heretofore could not be treated accurately with the Eulerian approach.


*Keywords:* Quadrature method of moments; Number density function; Kinetic equation; Fluid-particle flows; Multiphase systems

## 1. Introduction

The direct quadrature method of moments (DQMOM) is an efficient Eulerian formulation for describing polydisperse multiphase flows [20]. It is especially useful for treating dense sprays undergoing coalescence, and for submicron particulate/aerosol systems subject to Brownian aggregation [27,22]. In comparison, standard moment methods have great difficulty treating systems with aggregation/coalescence and breakage. For other processes (e.g. evaporation, drag) the DQMOM equations are equivalent to the widely used Lagrangian

* Corresponding author. Tel.: +1 515 294 9104; fax: +1 515 294 2689.
*E-mail address:* rofox@iastate.edu (R.O. Fox).

0021-9991/$ - see front matter © 2007 Elsevier Inc. All rights reserved.
doi:10.1016/j.jcp.2007.10.026

particle method for sprays [6]. However, even when used in this context, DQMOM has the inherent advantage over Lagrangian methods of precisely controlling the statistical noise in the lower-order moments (e.g. droplet number density, mass density, Sauter radius). For a given desired accuracy, this greatly reduces the computational cost since a large number of numerical particles is not required to eliminate statistical noise [4].

In previous work, the advantages of using DQMOM for treating particle populations with low Stokes numbers (i.e., the dispersed-phase velocity follows closely the velocity of the continuous phase) have been clearly demonstrated [21,22,35,38]. These models have been implemented in flow codes for treating the formation of nanoparticles (e.g. soot) in flames, colloidal aggregation in liquids, and aerosols in the atmosphere. For these applications, the DQMOM transport equations take the form of standard scalar transport equations and are thus easily added to existing flow codes. The treatment of a dispersed-phase with finite Stokes number introduces the additional complication of accounting for the dispersed-phase velocity (and its dependence on particle size). In the Lagrangian formulation, this is done by solving for the particle velocity as it traverses the (Eulerian) gas phase. In quadrature methods, it is done by solving an Eulerian model where each quadrature node has it own velocity field.

In order to test the validity of the quadrature methods for sprays, the laminar nozzle-flow problem described in [18] has been recently investigated [14] using both DQMOM and Lagrangian particle tracking. This problem is particularly challenging due to the significant coalescence rates caused by droplets of different sizes having very different Stokes numbers (and hence different velocities). Nevertheless, the comparison between the two methods showed excellent agreement between quantities such as the droplet number density, mass density and Sauter radius. The computational cost for DQMOM was however two orders of magnitude lower than the Lagrangian method. This result is very promising and motivates our interest in developing the model further. The previous work on quadrature methods has identified two important points requiring further study [14]: (i) the treatment of non-linear evaporation, and (ii) the treatment of velocity dispersion in the context of moment closures. The second point is the topic investigated in this work.

As an example, consider a laminar spray. The Williams equation [36] for the joint volume ($v$), velocity ($\mathbf{v}$) number density function $f(t,\mathbf{x},v,\mathbf{v})$ is

$$\partial_t f + \mathbf{v}\cdot\partial_{\mathbf{x}} f + \partial_v(R_v f) + \partial_{\mathbf{v}}\cdot\left(f\frac{\mathbf{F}}{m_{\mathrm{p}}}\right) = Q, \tag{1}$$

where $R_v$ is the evaporation rate, $\mathbf{F}$ is the drag force acting on a droplet, $m_{\mathrm{p}}$ is the droplet mass, and $Q$ is the collisions/coalescence term.[1] Note that the number density function has four degrees of freedom (one for $v$ and three for $\mathbf{v} = [v_1, v_2, v_3]^{\mathrm{T}}$), and it is intractable to solve directly for realistic fluid-particle flows using an Eulerian sectional method that discretizes $v$–$\mathbf{v}$ phase space [1]. In most application codes (1) is approximated using a Lagrangian method [6,4]. Although straightforward to implement numerically, this method does require a relatively large number of "parcels" to represent the spray in order to control statistical noise and bias. Note that extending $f$ to include other variables (e.g. droplet temperature, chemical composition, etc.) is straightforward if the appropriate rate expressions are added to (1).

Classical moment closures for (1) start by defining the moments of $f$:

$$\left\langle v^k v_1^l v_2^m v_3^p \right\rangle \equiv \int_{-\infty}^{+\infty}\int_0^{\infty} v^k v_1^l v_2^m v_3^p f(v,\mathbf{v})\,\mathrm{d}v\,\mathrm{d}\mathbf{v}, \tag{2}$$

where the usual practice is to consider only non-negative integers for $k$–$p$. Applying the moment transformation to (1) leads to a transport equation for the moments:

$$\partial_t\left\langle v^k v_1^l v_2^m v_3^p\right\rangle + \partial_{\mathbf{x}}\cdot\left\langle v^k v_1^l v_2^m v_3^p \mathbf{v}\right\rangle = \int_{-\infty}^{+\infty}\int_0^{\infty} v^k v_1^l v_2^m v_3^p P\,\mathrm{d}v\,\mathrm{d}\mathbf{v}, \tag{3}$$

where $P$ denotes the terms for evaporation, drag, and coalescence. In general, only the first term in Eq. (3) is closed. The second term describes spatial transport and contains moments one order higher in velocity:

[1] Collisions leave the particle volumes unchanged, but modify the velocities. Coalescence implies a change in particle volumes.

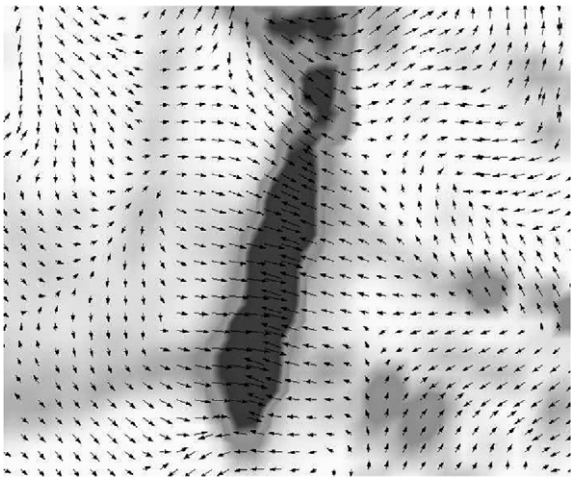

Fig. 1. Particle velocity variance found from a Lagrangian simulation in isotropic turbulence with finite Stokes number. Arrows indicate the direction of the most compressive strain rate of the fluid velocity. Regions of high variance are generated where the particles are unable to decelerate as quickly as the fluid, leading to particle-crossing trajectories.

$$\left\langle v^k v_1^l v_2^m v_3^p \mathbf{v} \right\rangle = \begin{bmatrix} \left\langle v^k v_1^{l+1} v_2^m v_3^p \right\rangle \\ \left\langle v^k v_1^l v_2^{m+1} v_3^p \right\rangle \\ \left\langle v^k v_1^l v_2^m v_3^{p+1} \right\rangle \end{bmatrix}, \tag{4}$$

and it is never closed. In contrast, the term on the right-hand side of (3) will be closed at best only when the rate expressions for evaporation, drag, and coalescence are linear in $v$ and $\mathbf{v}$.

The closure of the right-hand side of (3) using quadrature methods is investigated in detail elsewhere [14], and so our primary focus here will be on closures for the spatial transport term. We are particularly interested in the performance of quadrature methods for non-equilibrium flows wherein the velocity density function is far from Maxwellian. For example, dilute systems often exhibit non-equilibrium behavior because particle collisions are too weak to overcome kinetic effects. In many cases the velocity density function can be non-unimodal, implying that there is a high probability of finding particles with distinctly different velocities at the same location. In Lagrangian simulations of dilute systems, such behavior can be easily captured and is known as particle-trajectory crossing (PTC). In general, PTC does not occur at zero Stokes number because the fluid velocity is mono-kinetic [24]. However, beyond a critical Stokes number the particles are no longer able to follow the fluid and PTC can occur. Fig. 1 illustrates this phenomenon for finite Stokes number particles in isotropic turbulence. As discussed in detail below, "standard" moment closures are unable to correctly describe particle clustering (as measured by the particle number density $n_p$) because they do not account correctly for PTC. Thus, the only available method for simulating accurately dilute gas-particle systems is Lagrangian particle tracking. As mentioned earlier, such statistical methods are not well suited for computing Eulerian statistics due to statistical noise. For example, the accurate prediction of $n_p(t, \mathbf{x})$ (e.g. sufficiently accurate to compute its energy spectrum in a homogeneous flow) requires tens of millions of Lagrangian particles and hence very long computing times [15]. In contrast, an accurate Eulerian description of $n_p(t, \mathbf{x})$ would require a fraction of the computing cost (e.g. comparable to the cost of solving for the fluid velocity.) Such an Eulerian description has not been previously reported and is the goal of the work described here.

## 2. Moment closures for fluid-particle flows

### 2.1. Basic principles and state of the art

For the sake of simplicity, we shall restrict our attention to the case of monodisperse particles without thermal and mass exchange with the fluid phase. Moreover, complex phenomena such as particle collisions,

secondary atomization or turbulent dispersion will not be considered hereinafter. We shall focus only on the basic ideas of moment methods, especially on the closure problem, which is at the core of our quadrature-based method for Eulerian gas-particle modeling. Finally, we note that although we focus on gas–solid flows, the basic fundamental problems associated with moment closures (or two-fluid models in general) arise in many other applications (e.g. bubble-laden flow [11,12]).

The starting point to derive moment models is the Williams equation, which governs the particle evolution at the kinetic level in a $d$-dimensional physical space with particle velocity $\mathbf{v}$ and position $\mathbf{x}$. All the relevant physics can in theory be included in this equation. In the very simple case of a non-evaporating ($R_v = 0$), monodisperse particulate phase (with no collisions, secondary atomization, nor turbulent dispersion), this equation reads

$$\frac{\partial f}{\partial t} + \nabla_{\mathbf{x}} \cdot (f\mathbf{v}) + \nabla_{\mathbf{v}} \cdot \left( f \frac{\mathbf{F}}{m_{\mathrm{p}}} \right) = 0 \tag{5}$$

with $f(t, \mathbf{x}, \mathbf{v})$ being the particle number density function in the phase space $\mathcal{E} = \mathbb{R}^d \times \mathbb{R}^d$, $m_{\mathrm{p}}$ the mass of a particle, and $\mathbf{F}$ the force acting on a particle. If one assumes that the particle density is much greater than the fluid density (e.g. solid or liquid particles suspended in a gas), the expression for $\mathbf{F}$ is quite simple and corresponds (in an inertial frame) to the sum of the drag force and the gravity force (which is very often negligible). Hence one has

$$\mathbf{F}(\mathbf{U}_{\mathrm{f}}, \mathbf{v}) = \frac{1}{2} \pi r^2 \rho_{\mathrm{f}} C_{\mathrm{d}} |\mathbf{U}_{\mathrm{f}} - \mathbf{v}| (\mathbf{U}_{\mathrm{f}} - \mathbf{v}) + m_{\mathrm{p}} \mathbf{g},$$

where $\mathbf{U}_{\mathrm{f}}$ is the fluid velocity, $r$ is the particle radius, $\rho_{\mathrm{f}}$ the fluid density, and $C_{\mathrm{d}}$ is the particle drag coefficient given by the following correlation due to Schiller and Nauman [33]:

$$C_{\mathrm{d}} = \frac{24}{Re_{\mathrm{p}}} \left( 1 + \frac{1}{6} Re_{\mathrm{p}}^{2/3} \right),$$

with $Re_{\mathrm{p}} = 2|\mathbf{U}_{\mathrm{f}} - \mathbf{v}| r / \nu_{\mathrm{f}}$ being the particle Reynolds number where $\nu_{\mathrm{f}}$ is the fluid kinematic viscosity.

Let us now introduce the velocity moments up to fourth order:

$$\begin{aligned}
&M^0(t, \mathbf{x}) = \int_{\mathbb{R}^d} f(t, \mathbf{x}, \mathbf{v}) \mathrm{d}\mathbf{v}, \quad M^1_i(t, \mathbf{x}) = \int_{\mathbb{R}^d} v_i f(t, \mathbf{x}, \mathbf{v}) \mathrm{d}\mathbf{v}, \\
&M^2_{ij}(t, \mathbf{x}) = \int_{\mathbb{R}^d} v_i v_j f(t, \mathbf{x}, \mathbf{v}) \mathrm{d}\mathbf{v}, \quad M^3_{ijk}(t, \mathbf{x}) = \int_{\mathbb{R}^d} v_i v_j v_k f(t, \mathbf{x}, \mathbf{v}) \mathrm{d}\mathbf{v}, \\
&M^4_{ijkl}(t, \mathbf{x}) = \int_{\mathbb{R}^d} v_i v_j v_k v_l f(t, \mathbf{x}, \mathbf{v}) \mathrm{d}\mathbf{v},
\end{aligned}$$

with $\mathrm{d}\mathbf{v} = \mathrm{d}v_1 \ldots \mathrm{d}v_d$. Starting from (5) a straightforward calculation yields the following set of equations:

$$\begin{aligned}
&\frac{\partial M^0}{\partial t} + \frac{\partial M^1_l}{\partial x_l} = 0, \\
&\frac{\partial M^1_i}{\partial t} + \frac{\partial M^2_{il}}{\partial x_l} = g_i M^0 + \int_{\mathbb{R}^d} \frac{F_i}{m_{\mathrm{p}}} f \, \mathrm{d}\mathbf{v}, \\
&\frac{\partial M^2_{ij}}{\partial t} + \frac{\partial M^3_{ijl}}{\partial x_l} = g_i M^1_j + g_j M^1_i + \int_{\mathbb{R}^d} \left( v_j \frac{F_i}{m_{\mathrm{p}}} + v_i \frac{F_j}{m_{\mathrm{p}}} \right) f \, \mathrm{d}\mathbf{v}, \\
&\frac{\partial M^3_{ijk}}{\partial t} + \frac{\partial M^4_{ijkl}}{\partial x_l} = g_i M^2_{jk} + g_j M^2_{ik} + g_k M^2_{ij} + \int_{\mathbb{R}^d} \left( v_j v_k \frac{F_i}{m_{\mathrm{p}}} + v_i v_k \frac{F_j}{m_{\mathrm{p}}} + v_i v_j \frac{F_k}{m_{\mathrm{p}}} \right) f \, \mathrm{d}\mathbf{v},
\end{aligned} \tag{6}$$

where we have used the Einstein convention of implicit summation on repeated indices. It is clear that this system is not closed because of the drag terms on the right-hand side (rhs) and the presence of moments of order $n+1$ on the left-hand side (lhs) of the equation corresponding to the moment of order $n$. The most rigorous way to close the system is to make an assumption on the shape of the number density function. The simplest one (valid only for very small Stokes numbers) reads [17]:

$$f(t,\mathbf{x},\mathbf{v}) = n_{\mathrm{p}}(t,\mathbf{x})\delta_{\mathbf{v}-\mathbf{U}_{\mathrm{p}}(t,\mathbf{x})}, \tag{7}$$

$n_{\mathrm{p}}$ being the number of particles per unit volume and $\mathbf{U}_{\mathrm{p}}$ the mean particle velocity. For this choice, $f$ is fully determined by its first $1+d$ moments according to the following relations:

$$M^0(t,\mathbf{x}) = n_{\mathrm{p}}(t,x), \quad M^1_i(t,\mathbf{x}) = n_{\mathrm{p}}(t,\mathbf{x})U_{\mathrm{p}i}(t,\mathbf{x}). \tag{8}$$

Thus, only $1+d$ equations are needed to obtain a closed model.

Inserting relations (8) into the first $1+d$ equations of system (6), one obtains the following system:

$$\begin{aligned} &\frac{\partial n_{\mathrm{p}}}{\partial t} + \frac{\partial n_{\mathrm{p}}U_{\mathrm{p}j}}{\partial x_j} = 0,\\ &\frac{\partial n_{\mathrm{p}}U_{\mathrm{p}i}}{\partial t} + \frac{\partial n_{\mathrm{p}}U_{\mathrm{p}i}U_{\mathrm{p}j}}{\partial x_j} = n_{\mathrm{p}}g_i + \frac{n_{\mathrm{p}}}{m_{\mathrm{p}}}F_i(\mathbf{U}_{\mathrm{f}},\mathbf{U}_{\mathrm{p}}). \end{aligned} \tag{9}$$

This set of equations – or its variants in the case of polydisperse, evaporating particles [18,9], or the Eulerian two-fluid approach used for bubble-laden flows [11,12] – is a commonly used Eulerian model for small Stokes number gas-particle flows. However, it suffers from a major drawback: by construction (see 7), it is not able to take into account the presence of particles with different velocities located at the same point. This can lead to unphysical results in the case of two crossing jets of particles (e.g. at Stokes only slightly greater than zero) or in the case of a jet of particles impinging on a wall. This limitation also leads to an overestimation of the preferential concentration of particles in low vorticity regions of turbulent flows. These problems are closely related to the ill-posedness of system (9) in the space of functions even only locally integrable. Actually, it has been proven [3] that for a very wide class of initial conditions, the solution of the pressure-less gas dynamics system, which corresponds to the lhs of system (9), is singular in the sense that $\mathbf{U}_{\mathrm{p}}$ is a discontinuous function and $n_{\mathrm{p}}$ is a measure-valued distribution with its singular part concentrated on the discontinuities of the velocity field. In numerical applications, this means that $n_{\mathrm{p}}$ may become locally infinite, which in turn can result in numerical stiffness problems. Similar difficulties arise with the two-fluid model for bubble-laden flows [12]. The net result is that all multiphase models based on only two Eulerian moments (i.e., $n_{\mathrm{p}}$ and $\mathbf{U}_{\mathrm{p}}$) are bound to fail at reproducing Lagrangian statistics in non-equilibrium flows.

Another well-known problem with system (9) is that it is not able to reproduce the spreading of particles by turbulence, even if it is coupled to a turbulence model for the fluid. This problem can be partially solved by replacing the closure hypothesis (7) by a Gaussian-shape assumption (see e.g. [32] for related work):

$$f(t,\mathbf{x},\mathbf{v}) = \frac{n_{\mathrm{p}}(t,\mathbf{x})}{(2\pi\sigma_{\mathrm{p}}(t,\mathbf{x}))^{d/2}}\exp\left(\frac{|\mathbf{v}-\mathbf{U}_{\mathrm{p}}(t,\mathbf{x})|^2}{2\sigma_{\mathrm{p}}(t,\mathbf{x})^2}\right), \tag{10}$$

where $\sigma_{\mathrm{p}}$ is particle velocity standard deviation, and by introducing additional diffusion terms in the governing kinetic equation (see for example the work of Reeks [30] or Zaichik [37]). The simplest such model reads

$$\frac{\partial f}{\partial t} + \nabla_{\mathbf{x}}\cdot(f\mathbf{v}) + \nabla_{\mathbf{v}}\cdot\left(f\frac{\mathbf{F}}{m_{\mathrm{p}}}\right) - \nabla_{\mathbf{v}}\cdot(D\nabla_{\mathbf{v}}f) = 0, \tag{11}$$

where $D$ is a positive coefficient depending upon the properties of the fluid turbulence (turbulent kinetic energy and integral time scale). Taking the moments of (11) and using the closure relation (10), one obtains the following second-order Eulerian model for the particle dynamics:

$$\begin{aligned} &\frac{\partial n_{\mathrm{p}}}{\partial t} + \frac{\partial n_{\mathrm{p}}U_{\mathrm{p}j}}{\partial x_j} = 0,\\ &\frac{\partial n_{\mathrm{p}}U_{\mathrm{p}i}}{\partial t} + \frac{\partial n_{\mathrm{p}}U_{\mathrm{p}i}U_{\mathrm{p}j}}{\partial x_j} + \frac{\partial n_{\mathrm{p}}\sigma_{\mathrm{p}}^2}{\partial x_i} = n_{\mathrm{p}}g_i + \frac{n_{\mathrm{p}}}{(2\pi\sigma_{\mathrm{p}})^{d/2}}\int_{\mathbb{R}^d}\frac{F_i}{m_{\mathrm{p}}}\exp\left(\frac{|\mathbf{v}-\mathbf{U}_{\mathrm{p}}|^2}{2\sigma_{\mathrm{p}}^2}\right)\mathrm{d}\mathbf{v},\\ &\frac{\partial n_{\mathrm{p}}E_{\mathrm{p}}}{\partial t} + \frac{\partial (n_{\mathrm{p}}E_{\mathrm{p}} + n_{\mathrm{p}}\sigma_{\mathrm{p}}^2)U_{\mathrm{p}j}}{\partial x_j} = \mathbf{g}\cdot\mathbf{U}_{\mathrm{p}} + \frac{d}{2}n_{\mathrm{p}}D + \frac{n_{\mathrm{p}}}{(2\pi\sigma_{\mathrm{p}})^{d/2}}\int_{\mathbb{R}^d}\frac{\mathbf{F}\cdot\mathbf{v}}{m_{\mathrm{p}}}\exp\left(\frac{|\mathbf{v}-\mathbf{U}_{\mathrm{p}}|^2}{2\sigma_{\mathrm{p}}^2}\right)\mathrm{d}\mathbf{v}, \end{aligned} \tag{12}$$

where $E_p = 1/2|\mathbf{U}_p|^2 + (d/2)\sigma_p^2$ denotes the total kinetic energy of the particulate phase per unit mass. This system is very close to the compressible gas dynamics system, the term $\pi_p = n_p\sigma_p^2$ playing the role of a granular pressure. For strictly positive values of $\pi_p$, this system is hyperbolic and its solution, even discontinuous, always belongs to a space of functions and never contains a singular-measure-valued part. Nevertheless, in many applications, the pressure term remains weak compared to the inertial term (especially in the laminar part of the flow), and the singular behavior of the pressure-less gas dynamics system is not fully eliminated [15,24,4]. Moreover, because of closure assumption (10), this system is not adapted to reproduce strongly non-equilibrium situations such as those already mentioned (jet crossing, jet-wall interaction) and leads in those cases to non-physical solutions. For example, in the jet-crossing problem second-order closures such as (12) will generate effective particle "collisions" even though such terms do not appear in (1). This is the principal reason why we are motivated to seek a more general quadrature-based closure assumption, and to derive the corresponding moment model.

### 2.2. Quadrature-based moment closures

The quadrature method of moments (QMOM) was introduced by McGraw [27] as an efficient, yet accurate closure for univariate density functions $f(x)$. The principal idea is related to Gaussian quadrature, and can be expressed as

$$\int_0^\infty g(x)f(x)\mathrm{d}x = \sum_{\alpha=1}^{N} w_\alpha g(x_\alpha), \tag{13}$$

where $g(x)$ is an arbitrary smooth function. The non-negative weights $w_\alpha$ and abscissas $x_\alpha$ are determined from a system of non-linear equations:

$$\langle x^k \rangle = \sum_{\alpha=1}^{N} w_\alpha x_\alpha^k, \quad k \in \{0, 1, \ldots, 2N-1\}, \tag{14}$$

where the moments $\langle x^k \rangle$ are assumed to be known. This system can be solved accurately using the product-difference (PD) algorithm described elsewhere [27]. The basic computational algorithm then consists of solving transport equations for $\langle x^k \rangle$ ($k \in \{0, 1, \ldots, 2N-1\}$) wherein all non-linear terms are closed using (13). The QMOM algorithm has been shown to yield accurate results for problems involving univariate density functions, including complex integro-differential expressions arising from aggregation and breakage terms [22].

The extension of QMOM to multivariate problems is challenging because the PD algorithm cannot normally be used with more than one variable (this is related to the fact that there does not exist a Gaussian quadrature theory for arbitrary multi-dimensional functions). However, it is sometimes possible to solve the multi-variate version of (14) for a selected set of moments, and this is the procedure employed in this work.

The direct quadrature method of moments (DQMOM) consists of reinterpreting (13) as a closure assumption for (1) based on an expansion of the number density function in a sum of weighted delta functions in phase space [13,20,14]:

$$f(t, \mathbf{x}, \mathbf{v}) = \sum_{\alpha=1}^{N} n_\alpha \delta_{\mathbf{v}-\mathbf{U}_\alpha}, \tag{15}$$

where $\delta_{\mathbf{v}-\mathbf{U}_\alpha} \equiv \delta_{v_1-U_{\alpha 1}}\delta_{v_2-U_{\alpha 2}}\delta_{v_3-U_{\alpha 3}}$. The approximation in (15) is similar to the Lagrangian method, excepted that here the weights $n_\alpha$ and abscissas ($\mathbf{U}_\alpha = [U_{\alpha 1}, U_{\alpha 2}, U_{\alpha 3}]^{\mathrm{T}}$) are fields. Thus we can interpret $n_\alpha$ to be the weights of parcels ($n_\alpha$ has units of number of particles per unit volume), and $\mathbf{U}_\alpha$ to be the corresponding velocity. Application of DQMOM to (1) results in transport equations for the number density and momentum density of each quadrature node [14]. In principal, these equations could be solved with appropriate initial and boundary conditions to find the fields $n_\alpha(t, \mathbf{x})$ and $\mathbf{U}_\alpha(t, \mathbf{x})$ appearing in (15). However, this procedure in itself is not sufficient to avoid singularities of the type inherent in (9).

The quadrature approximation for the moments of a multi-variate number density function are found directly from (15):

$$\left\langle v_1^l v_2^m v_3^p \right\rangle = \sum_{\alpha=1}^{N} n_\alpha U_{\alpha 1}^l U_{\alpha 2}^m U_{\alpha 3}^p. \tag{16}$$

The fundamental idea behind quadrature methods is that we should choose the weights and abscissas such that as many moments as possible agree with moment transport equations found from the kinetic equation. Note that there are a total of $N$ weights and $3N$ abscissas. We will thus need to choose an equal number of independent moments to determine the weights and abscissas. Note that in the limit of small Stokes numbers $\mathbf{U}_\alpha$ can be replaced by the continuous-phase velocity $\mathbf{U}_\mathrm{f}$. However, our primary interest in this work is the behavior of quadrature methods for finite Stokes numbers where $\mathbf{U}_\alpha$ is not equal to the continuous-phase velocity.

### 2.3. A two-node quadrature-based moment closure

In this work we will consider the following two-node closure hypothesis [8]:

$$f(t,\mathbf{x},\mathbf{v}) = n_1(t,\mathbf{x})\delta_{\mathbf{v}-\mathbf{U}_1(t,\mathbf{x})} + n_2(t,\mathbf{x})\delta_{\mathbf{v}-\mathbf{U}_2(t,\mathbf{x})}. \tag{17}$$

This is a direct generalization of closure relation (7) that is motivated by DQMOM. This new distribution is fully characterized by $2+2d$ degrees of freedom. It is thus natural to build a model corresponding to the conservation of $2+2d$ moments. For both simplicity and symmetry reasons, we have chosen to work with the following set of moments:

$$\begin{aligned} &M^0 = n_1 + n_2, \quad M_i^1 = n_1 U_{1i} + n_2 U_{2i}, \\ &M_{ii}^2 = n_1 U_{1i}^2 + n_2 U_{2i}^2, \quad Q = \sum_{i=1}^{d} M_{iii}^3 = \sum_{i=1}^{d} \left( n_1 U_{1i}^3 + n_2 U_{2i}^3 \right). \end{aligned} \tag{18}$$

Inserting these expressions into system (6) and using (17), an easy calculation yields a system of $2(1+d)$ moment equations:

$$\begin{aligned} &\frac{\partial M^0}{\partial t} + \frac{\partial M_i^1}{\partial x_i} = 0, \\ &\frac{\partial M_1^1}{\partial t} + \frac{\partial M_{1i}^2}{\partial x_i} = g_1 M^0 + \frac{n_1}{m_\mathrm{p}} F_1(\mathbf{U}_\mathrm{f},\mathbf{U}_1) + \frac{n_2}{m_\mathrm{p}} F_1(\mathbf{U}_\mathrm{f},\mathbf{U}_2), \\ &\vdots \\ &\frac{\partial M_d^1}{\partial t} + \frac{\partial M_{di}^2}{\partial x_i} = g_d M^0 + \frac{n_1}{m_\mathrm{p}} F_d(\mathbf{U}_\mathrm{f},\mathbf{U}_1) + \frac{n_2}{m_\mathrm{p}} F_d(\mathbf{U}_\mathrm{f},\mathbf{U}_2), \\ &\frac{\partial M_{11}^2}{\partial t} + \frac{\partial M_{11i}^3}{\partial x_i} = 2 g_1 M_1^1 + 2\frac{n_1}{m_\mathrm{p}} U_{11} F_1(\mathbf{U}_\mathrm{f},\mathbf{U}_1) + 2\frac{n_2}{m_\mathrm{p}} U_{21} F_1(\mathbf{U}_\mathrm{f},\mathbf{U}_2), \\ &\vdots \\ &\frac{\partial M_{dd}^2}{\partial t} + \frac{\partial M_{ddi}^3}{\partial x_i} = 2 g_d M_d^1 + 2\frac{n_1}{m_\mathrm{p}} U_{1d} F_d(\mathbf{U}_\mathrm{f},\mathbf{U}_1) + 2\frac{n_2}{m_\mathrm{p}} U_{2d} F_d(\mathbf{U}_\mathrm{f},\mathbf{U}_2), \\ &\frac{\partial Q}{\partial t} + \frac{\partial R_i}{\partial x_i} = 3\sum_{j=1}^{d} \left( g_j M_{jj}^2 + \frac{n_1}{m_\mathrm{p}} U_{1j}^2 F_j(\mathbf{U}_\mathrm{f},\mathbf{U}_1) + \frac{n_2}{m_\mathrm{p}} U_{2j}^2 F_j(\mathbf{U}_\mathrm{f},\mathbf{U}_2) \right), \end{aligned} \tag{19}$$

with $R$, $M_{ij}^2$ and $M_{iij}^3$ given by the following expressions (resulting from their definitions and the closure assumption on $f$):

$$M^2_{ij} = n_1 U_{1i} U_{1j} + n_2 U_{2i} U_{2j}, \quad M^3_{iij} = n_1 U^2_{1i} U_{1j} + n_2 U^2_{2i} U_{2j},$$
$$R_i = n_1 \left( \sum_{j=1}^{d} U^3_{1j} \right) U_{1i} + n_2 \left( \sum_{j=1}^{d} U^3_{2j} \right) U_{2i}.$$

For system (19) to be closed (and well defined), it is necessary to prove that for any given admissible state

$$W = \left( M^0, M^1_1, \ldots, M^1_d, M^2_{11}, \ldots, M^2_{dd}, Q \right) \in \mathbb{R}^{2+2d},$$

there exists one pair

$$V = [(n_1, \mathbf{U}_1), (n_2, \mathbf{U}_2)] \in \mathbb{R}^{1+d} \times \mathbb{R}^{1+d},$$

such that relations (18) are fulfilled. This is the object of the following proposition.

**Proposition 2.1.** *Let*

$$W = \left( M^0, M^1_1, \ldots, M^1_d, M^2_{11}, \ldots, M^2_{dd}, Q \right) \in \mathbb{R}^{2+2d},$$

*such that*

$$\text{(i)} \quad M^0 > 0 \quad \text{and} \quad (ii) \quad \forall i = 1, \ldots, d \quad M^0 M^2_{ii} \geqslant (M^1_i)^2.$$

Up to a permutation between the subscripts 1 and 2, there exists only one solution $V = [(n_1, \mathbf{U}_1), (n_2, \mathbf{U}_2)] \in \mathbb{R}^{1+d} \times \mathbb{R}^{1+d}$, which is not modified by permuting the axis of the referential frame and which fulfills the consistency relations (18). It is given by

$$\begin{aligned} &n_1 = (1/2 + x) M^0, \quad n_2 = (1/2 - x) M^0, \\ &U_{1i} = U_{\mathrm{p}i} - \left( \frac{n_2}{n_1} \right)^{1/2} \sigma_{\mathrm{p}i}, \quad U_{2i} = U_{\mathrm{p}i} + \left( \frac{n_1}{n_2} \right)^{1/2} \sigma_{\mathrm{p}i}, \end{aligned} \tag{20}$$

with

$$x = \frac{q_{\mathrm{p}}/2}{\left( q^2_{\mathrm{p}} + 4 \left( \sum_{i=1}^{d} \sigma^3_{\mathrm{p}i} \right)^2 \right)^{1/2}},$$

and where $U_{\mathrm{p}i}$, $\sigma_{\mathrm{p}i}$ and $q_{\mathrm{p}}$ are defined by

$$U_{\mathrm{p}i} = \frac{M^1_i}{M^0}, \quad \sigma_{\mathrm{p}i} = \left( \frac{M^0 M^2_{ii} - (M^1_i)^2}{(M^0)^2} \right)^{1/2},$$
$$q_{\mathrm{p}} = \frac{1}{M^0} \left( Q - M^0 \sum_{i=1}^{d} U^3_{\mathrm{p}i} - 3 M^0 \sum_{i=1}^{d} \sigma^2_{\mathrm{p}i} U_{\mathrm{p}i} \right).$$

Hereinafter, it will be implicitly assumed that the mapping $W \to V$ is defined by (20). As it will be shown in the proof below, this solution is in general not the only one possible (except when $d = 1$). This is due to the non-invariance under rotation of model (19). Nevertheless, this solution is the most "natural" one since it is the only one that is invariant under axis permutation.

**Proof of Proposition 2.1.** First, thanks to conditions (i) and (ii), we note that for all $i \in \{1, \ldots, d\}$, $\sigma_{\mathrm{p}i}$ is a real positive number. Then, using the notation introduced above, we can check easily that system (18) is equivalent to the following:

$$
\begin{aligned}
&n_1 = (1/2+x)M^0, \quad n_2 = (1/2-x)M^0,\\
&(1/2+x)\delta U_{1i} + (1/2-x)\delta U_{1i} = 0 \quad \forall i = 1,\dots,d,\\
&(1/2+x)(\delta U_{1i})^2 + (1/2-x)(\delta U_{2i})^2 = \sigma_{\mathrm{p}i}^2 \quad \forall i = 1,\dots,d,\\
&(1/2+x)(\delta U_{1i})^3 + (1/2-x)(\delta U_{2i})^3 = q_{\mathrm{p}},
\end{aligned}
\tag{21}
$$

with $\delta\mathbf{U}_1 = \mathbf{U}_1 - \mathbf{U}_{\mathrm{p}}$ and $\delta\mathbf{U}_2 = \mathbf{U}_2 - \mathbf{U}_{\mathrm{p}}$. A straightforward calculation yields

$$
\begin{aligned}
&n_1 = (1/2+x)M^0, \quad n_2 = (1/2-x)M^0,\\
&\delta U_{11} = -\varepsilon_1\left(\frac{1/2-x}{1/2+x}\right)^{1/2}\sigma_{\mathrm{p}1}, \quad \delta U_{21} = \varepsilon_1\left(\frac{1/2+x}{1/2-x}\right)^{1/2}\sigma_{\mathrm{p}1},\\
&\vdots\\
&\delta U_{1d} = -\varepsilon_d\left(\frac{1/2-x}{1/2+x}\right)^{1/2}\sigma_{\mathrm{p}d}, \quad \delta U_{2d} = \varepsilon_d\left(\frac{1/2+x}{1/2-x}\right)^{1/2}\sigma_{\mathrm{p}d},\\
&(1/2+x)\sum_{i=1}^{d}(\delta U_{1i})^3 + (1/2-x)\sum_{i=1}^{d}(\delta U_{2i})^3 = q_{\mathrm{p}},
\end{aligned}
\tag{22}
$$

with $\varepsilon_1 = \pm 1,\dots,\varepsilon_d = \pm 1$. Inserting the expressions for $\delta\mathbf{U}_1$ and $\delta\mathbf{U}_2$ into the last equation yields the following equation for $x$:

$$
-(1/2-x)^2 s_{\mathrm{p}} + (1/2+x)^2 s_{\mathrm{p}} = (1/4-x^2)^{1/2} q_{\mathrm{p}}.
$$

where $s_{\mathrm{p}} = \sum_{i=1}^{d}\varepsilon_i\sigma_{\mathrm{p}i}^3$. An easy calculation yields

$$
2s_{\mathrm{p}}x = q_{\mathrm{p}}(1/4-x^2)^{1/2}. \tag{23}
$$

Then (23) implies that

$$
\left(4s_{\mathrm{p}}^2 + q_{\mathrm{p}}^2\right)x^2 = \frac{1}{4}q_{\mathrm{p}}^2, \tag{24}
$$

which finally yields

$$
x = \mathrm{sign}(s_{\mathrm{p}})\frac{q_{\mathrm{p}}}{2\left(q_{\mathrm{p}}^2 + 4s_{\mathrm{p}}^2\right)^{1/2}}. \tag{25}
$$

If all $\varepsilon_i$ are of the same sign, condition (ii) of Proposition 2.1 ensures that $x$ is well defined and lies in $]-1/2, 1/2[$ for all $q_{\mathrm{p}}$. On the contrary, in cases where all $\varepsilon_i$ do not have the same sign, it is necessary to assume that $s_{\mathrm{p}} \neq 0$ to ensure that $|x| \neq 1/2$ for all $q_{\mathrm{p}}$, but this hypothesis has no physical meaning and strongly depends on the choice of the reference frame. This is the reason why only the solutions corresponding to the choice $\varepsilon_1 = \varepsilon_2 = \cdots = \varepsilon_d = 1$ or $\varepsilon_1 = \varepsilon_2 = \cdots = \varepsilon_d = -1$ have to be considered here as admissible solutions.

Coming back to (22), it is easy to check that these two possible solutions are actually the same up to a permutation of $(n_1, \mathbf{U}_1)$ with $(n_2, \mathbf{U}_2)$. This concludes the proof. □

## 3. Numerical scheme

Because of the conservative form of system (19), the finite-volume method [19] is a natural candidate for its discretization and the underlying kinetic equation (5) can be used for the derivation of a numerical flux formula that ensures the robustness of the corresponding scheme. For the sake of clarity, let us begin by considering the one-dimensional case, the multi-dimensional extension being straightforward. We will also show the equations in terms of the two-node quadrature closure. The equations for the one-node quadrature closure (i.e., system (9)) follow directly by simply eliminating the second node. We should note that stable numerical schemes for systems (9) and (19) must account for their fundamentally hyperbolic nature.

### 3.1. A first-order, one-dimensional scheme

For one space dimension, system (19) reads

$$\begin{aligned}
&\frac{\partial M^0}{\partial t}+\frac{\partial M^1}{\partial x}=0,\\
&\frac{\partial M^1}{\partial t}+\frac{\partial M^2}{\partial x}=gM^0+\frac{n_1}{m_\mathrm{p}}F(U_\mathrm{f},U_1)+\frac{n_2}{m_\mathrm{p}}F(U_\mathrm{f},U_2),\\
&\frac{\partial M^2}{\partial t}+\frac{\partial M^3}{\partial x}=2gM^1+2\frac{n_1}{m_\mathrm{p}}U_1F(U_\mathrm{f},U_1)+2\frac{n_2}{m_\mathrm{p}}U_2F(U_\mathrm{f},U_2),\\
&\frac{\partial M^3}{\partial t}+\frac{\partial M^4}{\partial x}=3gM^2+3\frac{n_1}{m_\mathrm{p}}U_1^2F(U_\mathrm{f},U_1)+3\frac{n_2}{m_\mathrm{p}}U_2^2F(U_\mathrm{f},U_2),
\end{aligned}\tag{26}$$

with $M^k=n_1U_1^k+n_2U_2^k$. Let us introduce the following notation:

$$W=\begin{pmatrix}M^0\\M^1\\M^2\\M^3\end{pmatrix},\quad H(W)=\begin{pmatrix}M^1\\M^2\\M^3\\M^4\end{pmatrix},\quad S(W)=\begin{pmatrix}0\\gM^0+\frac{n_1}{m_\mathrm{p}}F_1+\frac{n_2}{m_\mathrm{p}}F_2\\2gM^1+2\frac{n_1}{m_\mathrm{p}}U_1F_1+2\frac{n_2}{m_\mathrm{p}}U_2F_2\\3gM^2+3\frac{n_1}{m_\mathrm{p}}U_1^2F_1+3\frac{n_2}{m_\mathrm{p}}U_2^2F_2\end{pmatrix},$$

with $F_1=F(U_\mathrm{f},U_1)$ and $F_2=F(U_\mathrm{f},U_2)$. Using classical notation, a fractional two-step, first-order, explicit, finite-volume scheme for system (26) reads

$$\begin{aligned}
&W_i^*=W_i^n-\frac{\Delta t}{\Delta x}\left[G\left(W_i^n,W_{i+1}^n\right)-G\left(W_{i-1}^n,W_i^n\right)\right],\\
&W_i^{n+1}=\widetilde{W}\left(W_i^*,\Delta t\right),
\end{aligned}\tag{27}$$

where $G$ is the numerical flux function (defined below) and $\widetilde{W}\left(W_i^*,\Delta t\right)$ is an approximate solution at time $t=\Delta t$ of the differential system

$$\frac{\mathrm{d}W}{\mathrm{d}t}=S(W)\quad\text{with } W(0)=W_i^*.\tag{28}$$

The advantage of a fractional-step algorithm is the possibility of using a quasi-analytic solution for the second step of the scheme to handle the stiffness of the source term. To compute this solution, let us first remark that, after some algebra, system (28) is equivalent to the following:

$$\begin{aligned}
&\frac{\mathrm{d}n_1}{\mathrm{d}t}=0,\quad \frac{\mathrm{d}U_1}{\mathrm{d}t}=\frac{F(U_\mathrm{f},U_1)}{m_\mathrm{p}}+g,\\
&\frac{\mathrm{d}n_2}{\mathrm{d}t}=0,\quad \frac{\mathrm{d}U_2}{\mathrm{d}t}=\frac{F(U_\mathrm{f},U_2)}{m_\mathrm{p}}+g.
\end{aligned}\tag{29}$$

The drag force may be rewritten as

$$F(U_\mathrm{f},U_\mathrm{p})=m_\mathrm{p}\frac{U_\mathrm{f}-U_\mathrm{p}}{\tau_\mathrm{p}(U_\mathrm{f},U_\mathrm{p})},\tag{30}$$

where $\tau_\mathrm{p}$ stands for the particle dynamical response time and is given by

$$\tau_\mathrm{p}(U_\mathrm{f},U_\mathrm{p})=\frac{2\rho_\mathrm{p}r^2}{9\mu_\mathrm{f}}\left(1+\frac{1}{6}Re_\mathrm{p}^{2/3}\right).\tag{31}$$

Using a frozen expression for $\tau_p(U_\mathrm{f},U_\mathrm{p})$, system (29) can be explicitly solved. Setting $\tau_i=\tau_\mathrm{p}\left(U_\mathrm{f},U_i^*\right)$, it yields the following expression for $n_1^{n+1}$, $n_2^{n+1}$, $U_1^{n+1}$, and $U_2^{n+1}$:

$$\begin{aligned} n_1^{n+1} &= n_1^*, \\ n_2^{n+1} &= n_2^*, \\ U_1^{n+1} &= \exp(-\Delta t/\tau_1)U_1^* + [1-\exp(-\Delta t/\tau_1)](U_f + g\tau_1), \\ U_2^{n+1} &= \exp(-\Delta t/\tau_2)U_2^* + [1-\exp(-\Delta t/\tau_2)](U_f + g\tau_2), \end{aligned} \tag{32}$$

where $n_1^*,\ n_2^*,\ U_1^*,\ U_2^*$ can be deduced from $W^*$ thanks to the formulae of Proposition 2.1.

It remains to give the expression for the numerical flux $G$. Let us start from the kinetic origin of system (26). By construction, one has the following properties:

$$W = \int_{\mathbb{R}^d} K(v) f_W(v)\mathrm{d}v, \quad H(W) = \int_{\mathbb{R}^d} vK(v) f_W(v)\mathrm{d}v$$

with $K(v) = [1\ v\ v^2\ v^3]^{\mathrm{T}}$ and $f_W(v) = n_1\delta_{v-U_1} + n_2\delta_{v-U_2}$, where $n_1$, $n_2$, $U_1$, and $U_2$ are related to $W$ thanks to (20). Using the ideas of kinetic schemes [29,7,28,10], it is natural to adopt the following expression for the numerical flux function:

$$G(W_l, W_r) = \int_{\mathbb{R}} \frac{1}{2}(v+|v|)K(v) f_{W_l}(v)\mathrm{d}v + \int_{\mathbb{R}} \frac{1}{2}(v-|v|)K(v) f_{W_r}(v)\mathrm{d}v, \tag{33}$$

which formally corresponds to a splitting between particles going from left to right (first term), and particles going from right to left (second term). Inserting the expression for $f_W$ in (33) yields

$$G(W_l, W_r) = H^+(W_l) + H^-(W_r), \tag{34}$$

with

$$H^+(W_l) = n_{1l}\max(U_{1l}, 0)\begin{pmatrix} 1 \\ U_{1l} \\ U_{1l}^2 \\ U_{1l}^3 \end{pmatrix} + n_{2l}\max(U_{2l}, 0)\begin{pmatrix} 1 \\ U_{2l} \\ U_{2l}^2 \\ U_{2l}^3 \end{pmatrix}, \tag{35}$$

and

$$H^-(W_r) = n_{1r}\min(U_{1r}, 0)\begin{pmatrix} 1 \\ U_{1r} \\ U_{1r}^2 \\ U_{1r}^3 \end{pmatrix} + n_{2r}\min(U_{2r}, 0)\begin{pmatrix} 1 \\ U_{2r} \\ U_{2r}^2 \\ U_{2r}^3 \end{pmatrix}. \tag{36}$$

Since the definition of scheme Eqs. (27)–(32) involves the mapping $W \to V$, it is mandatory to verify that, under a suitable condition on the time-step, the constraints (i) and (ii) of Proposition 2.1 are fulfilled at time $t^{n+1}$, assuming that they are satisfied for each cell at time $t^n$. Let us denote by $\mathcal{W}_{\mathrm{ad}}$ the set of all admissible states, e.g.

$$\mathcal{W}_{\mathrm{ad}} = \{W \in R^4,\ W^1 > 0,\ W^3W^1 > (W^2)^2\}.$$

Actually, we have the following proposition.

**Proposition 3.1.** *If for all $i \in Z$, $W_i^n \in \mathcal{W}_{\mathrm{ad}}$ and if $\Delta t < \inf_{i\in Z} \frac{\Delta x}{\max(|U_{1i}^n|, |U_{2i}^n|)}$ the scheme*

$$W_i^* = W_i^n - \frac{\Delta t}{\Delta x}\left[G\left(W_i^n, W_{i+1}^n\right) - G\left(W_{i-1}^n, W_i^n\right)\right],$$

*with $G$ defined by (34)–(36), is such that $\forall i \in Z$, $W_i^* \in \mathcal{W}_{\mathrm{ad}}$.*

**Proof of Proposition 3.1.** Using the definition (33) of the numerical flux, the finite-volume scheme may be rewritten as

$$W_i^* = \int_{\mathbb{R}} K(v)\left[(1-\lambda|v|)f_{W_i^n}(v) + \lambda v^+ f_{W_{i-1}^n}(v) - \lambda v^- f_{W_{i+1}^n}(v)\right]\mathrm{d}v,$$

with $\lambda = \Delta t/\Delta x$, $v^+ = \max(v,0)$ and $v^- = \min(v,0)$. For $\Delta t$ satisfying the CFL condition $\lambda < \frac{1}{\max\left(\left|U^n_{1i}\right|,\left|U^n_{2i}\right|\right)}$, the velocity distribution

$$g(v) = (1-\lambda|v|)f_{W_i^n}(v) + \lambda v^+ f_{W^n_{i-1}}(v) - \lambda v^- f_{W^n_{i+1}}(v),$$

is obviously a non-negative measure on $\mathbb{R}$. Using this property, it is straightforward to prove [28,10] that $W_i^* = \int_{\mathbb{R}} K(v)g(v)\mathrm{d}v$ lies in $\mathcal{W}_{\mathrm{ad}}$. □

### 3.2. Second-order extension

We will now focus on the second-order extension in the case of one spatial dimension. The use of a Runge–Kutta type time integration allows us to increase the temporal accuracy to second-order easily. Indeed, a second-order Runge–Kutta can be seen as a full time-step advancement using a first-order Euler method followed by a second full time-step advancement using the solution interpolated at mid time-step to compute the time derivatives. As a result, one can still use the two-step fractional time integration (27) for each of the two Runge–Kutta steps. Recalling that we are solving for $W_i^{n+1}$, the temporal scheme consists of the following first step:

$$\begin{aligned} W_i^{**} &= W_i^n - \frac{\Delta t}{\Delta x}\left[G\left(W_i^n, W_{i+1}^n\right) - G\left(W_{i-1}^n, W_i^n\right)\right], \\ W_i^{*,n+1} &= \widetilde{W}\left(W_i^{**}, \Delta t\right). \end{aligned} \tag{37}$$

From the first-order estimate $W_i^{*,n+1}$, we can construct an estimate for the mid time-step value $W_i^{*,n+\frac{1}{2}}$ by

$$W_i^{*,n+\frac{1}{2}} = \frac{1}{2}\left(W_i^n + W_i^{*,n+1}\right). \tag{38}$$

We then apply the second step of the Runge–Kutta scheme to obtain the second-order accurate solution $W_i^{n+1}$:

$$\begin{aligned} W_i^{*} &= W_i^n - \frac{\Delta t}{\Delta x}\left[G\left(W_i^{*,n+\frac{1}{2}}, W_{i+1}^{*,n+\frac{1}{2}}\right) - G\left(W_{i-1}^{*,n+\frac{1}{2}}, W_i^{*,n+\frac{1}{2}}\right)\right], \\ W_i^{n+1} &= \widetilde{W}\left(W_i^{*}, \Delta t\right). \end{aligned} \tag{39}$$

We will now describe the procedure to obtain second-order spatial accuracy. This procedure is independent of the time discretization, therefore, we will drop the superscripts for the sake of clarity. The second-order spatial accuracy is achieved thanks to the MUSCL technique [34,5,19], where a piecewise linear reconstruction of the face values is used. In the computation of the numerical flux $G$, the values we use are the cell-face values, namely we compute the flux across the left face of cell $i$ with $G\left(W_{i-\frac{1}{2},-}, W_{i-\frac{1}{2},+}\right)$ and the flux across the right face of cell $i$ by $G\left(W_{i+\frac{1}{2},-}, W_{i+\frac{1}{2},+}\right)$. The face values of the solution are constructed by

$$\begin{aligned} W_{i-\frac{1}{2},-} &= W_{i-1} + \frac{1}{2}\phi(\rho_{i-1})(W_i - W_{i-1}), \\ W_{i-\frac{1}{2},+} &= W_i - \frac{1}{2}\phi(\rho_i)(W_{i+1} - W_i), \\ W_{i+\frac{1}{2},-} &= W_i + \frac{1}{2}\phi(\rho_i)(W_{i+1} - W_i), \\ W_{i+\frac{1}{2},+} &= W_{i+1} - \frac{1}{2}\phi(\rho_{i+1})(W_{i+2} - W_{i+1}), \end{aligned} \tag{40}$$

where the ratio $\rho$ between the upwinded and downwinded gradients is defined by

$$\rho_i = \frac{W_i - W_{i-1}}{W_{i+1} - W_i}, \tag{41}$$

and $\phi$ is a limiter. Indeed, the reconstruction without any limiter (i.e. $\phi = 1$) has the disadvantage of not being monotonous. In order to avoid introducing numerical oscillations by creating new local extrema, we need to use a limiting function $\phi$ that will gradually switch between stencils depending on the local smoothness of the numerical solution. Several options are available for $\phi$. We conducted numerical tests with the *min-mod*, *Van*

*Leer* and *Superbee* limiters [19]. The *Superbee* was found to give the best results, therefore it was used for all the second-order numerical simulations presented in the example section. Its expression reads

$$\phi(\rho) = \max(0, \min(2\rho, 1), \min(\rho, 2)). \tag{42}$$

Note that for the second-order scheme we have no formal proof that the moments will remain in $\mathcal{W}_{\text{ad}}$. Nevertheless, this is an important, but difficult point that we will leave to future work.

### 3.3. Multi-dimensional extension

The multi-dimensional extension of the scheme we just described follows naturally for finite volumes. Indeed, the quadrature formulae (20) have already been derived for multiple dimensions, and the computation of the right-hand side of system (19) in the multi-dimensional case is straightforward. The first step of the finite-volume scheme described by (27) will read

$$W_i^* = W_i^n - \frac{\Delta t}{V_i} \sum_{f \in \mathcal{F}} G\left(W_{f,-}^n, W_{f,+}^n, \mathbf{n}_f\right) A_f, \tag{43}$$

where $i$ is the control volume considered, and $f$ is one of the faces $\mathcal{F}$ of the control volume. $V_i$ is the volume of the cell $i$, and $A_f$ corresponds to the surface area of face $f$. $G\left(W_{f,-}^n, W_{f,+}^n, \mathbf{n}_f\right)$ is the numerical flux through the cell face $f$ defined by (34)–(36) where the face velocities used for the transport must now be taken to be $\mathbf{U}_{1/2,f,+/-} \cdot \mathbf{n}_f$.

## 4. Example applications

In this section, we apply the two-node quadrature closure to non-equilibrium fluid-particle flows in order to illustrate its ability to handle non-trivial problems. Because the drag term offers no particular closure problem, for clarity we will consider some cases without drag (or equivalently infinite Stokes). However, we shall see in other examples that the quadrature-based closure works satisfactorily over the entire range of Stokes numbers. Finally, in order to achieve good numerical resolution, we will use the second-order flux scheme to advance the moment equations whenever the problem is not one-dimensional. Additionally, it should be noted that in the quadrature step (20), the velocities can become infinite if $n_1$ or $n_2$ are identically zero. While there are a number of strategies to alleviate this problem, we simply chose to clip the value of $x$ between $[-0.49, 0.49]$. This basic technique did not seem to alter the accuracy of the results in any noticeable manner. However, as seen in the crossing particle jets example below, clipping does introduce a small amount of numerical dispersion. The choice of clipping values is the first we tried, and further experimentation might give slightly improved results. However, as shown in the following examples, this simple strategy already yields good results.

### 4.1. One-dimensional test case

#### 4.1.1. Impinging particles

The first flow that we consider is one-dimensional with two particle "packets" moving in opposite directions. The initial number density $n_{\text{p}}$ is shown in Fig. 2 ($t = 0$) where it can be seen that the packet on the left has number density one-half as large as that on the right. The initial average particle velocity $U_{\text{p}}$ is set to 1 for $x < 0.5$ and $-1$ for $x \geqslant 0.5$. The two packets will thus eventually "collide" as time advances. (Recall, however, that our particles are collision-less.) In terms of the moments, the initial conditions are

$$m_0 = n_{\text{p}}, \quad m_1 = n_{\text{p}} U_{\text{p}}, \quad m_2 = n_{\text{p}} U_{\text{p}}^2, \quad m_3 = n_{\text{p}} U_{\text{p}}^3,$$

which yields the following weights and abscissas for two-node quadrature:

$$w_1 = n_{\text{p}}/2, \quad w_2 = n_{\text{p}}/2, \quad U_1 = U_{\text{p}}, \quad U_2 = U_{\text{p}}.$$

We then apply the first-order numerical scheme described in Section 3 to advance the moments for both one-node and two-node quadrature.

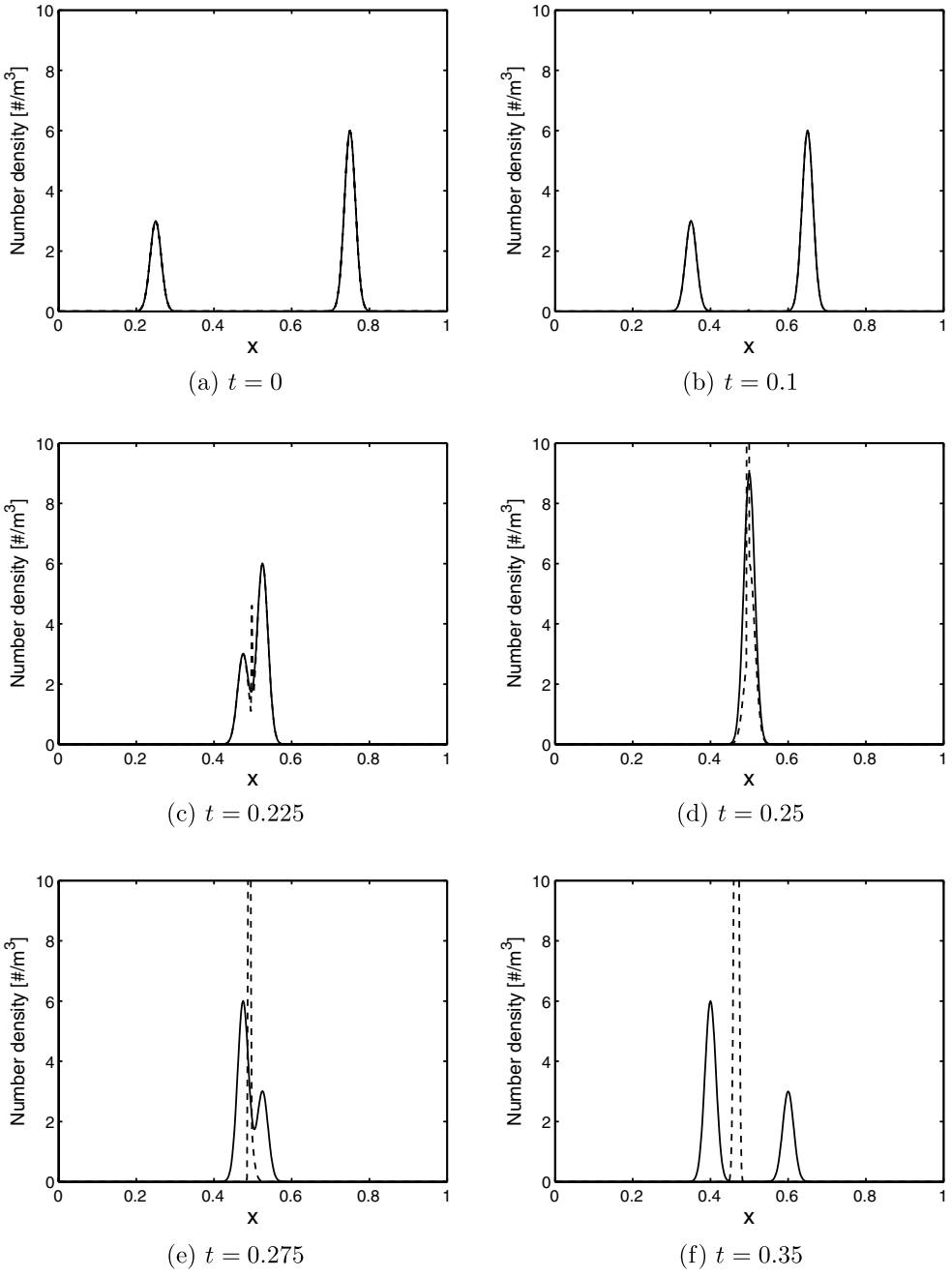


Fig. 2. Time evolution of number density for one-dimensional impinging particles. ---, one-node quadrature; —, two-node quadrature.

Fig. 2 illustrates the resulting time evolution of the particle number density. Before collision (i.e., before $n_p$ at $x = 0.5$ is greater than machine precision) both one-node and two-node quadrature yield identical results for $n_p$. However, as soon as $n_p$ becomes non-zero at $x = 0.5$ the two closures predict different values for all of the moments. With the one-node closure $n_p$ accumulates at $x = 0.5$ and the average velocity $U_p$ is independent of $t$. In contrast, with the two-node closure the two packets pass through each other and the average velocity (not shown) evolves in a non-trivial manner to finally end with $U_p$ equal $-1$ for $x < 0.5$ and 1 for $x \geqslant 0.5$ (i.e., the opposite sign compared to the initial conditions). Thus, the two-node closure yields a solution that exactly corresponds to the Lagrangian simulation of (1) in the limit of infinite Stokes.

The dramatic differences between the two closures is due to the fact that the two-node quadrature can describe particle-crossing trajectories, while the one-node closure cannot. Without this ability, a moment closure cannot predict any of the velocity moments (including the zero-order moment!) correctly for particles with Stokes numbers only slightly greater than zero and larger. We should note that second-order closures such as (12) also lack the ability to describe particle-crossing trajectories. This fact has important ramifications on the validity of using Eulerian multi-fluid models to investigate particle segregation in dilute fluid-particle flows (e.g. [16]) as a surrogate for Lagrangian methods. From this simple example, we can see that in general the segregation levels predicted by moment closures that cannot explicitly handle particle-crossing trajectories will be much larger than what would be found using a Lagrangian method.

### 4.2. Two-dimensional test cases

#### 4.2.1. Crossing particle jets

In this example, we demonstrate the ability of two-node quadrature to capture particle-crossing trajectories in two-dimensional flows with infinite Stokes number particles. The flow domain is the unit square and particle

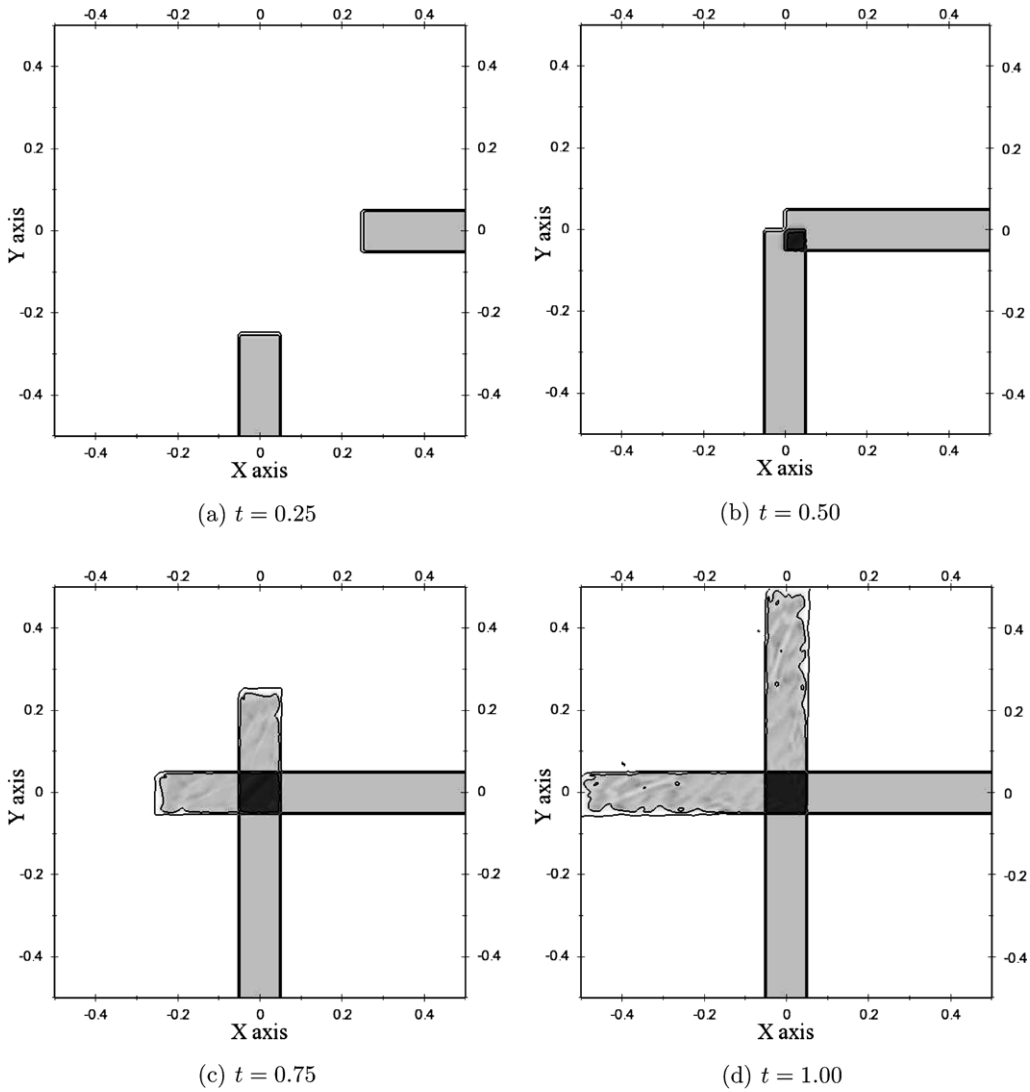


(a) $t = 0.25$ (b) $t = 0.50$

(c) $t = 0.75$ (d) $t = 1.00$

Fig. 3. Time evolution of particle number density for crossing jets.

jets are introduced centered at the bottom and right-hand sides of the domain with velocities of equal magnitude (see Fig. 3). The evolution of the particle number density is shown in Fig. 3. At early times ($t = 0.25$) the jets advance towards the center point. At $t = 0.50$, the jets begin to overlap and the local number density doubles. For subsequent times ($t = 0.75$), the jets continue along their original trajectories and finally exit ($t = 1.00$) the flow domain at the top and left-hand sides, respectively. We should note that if the second-order moment closure were used to compute this flow, the jets would "collide" at the center point and move off diagonally in one stream towards the upper left-hand corner of the domain (i.e., with a velocity equal to the average velocity of the two incoming jets). Just as in the previous example, the key to success is the fact that two-node quadrature can describe the bimodal velocity distribution that occurs in the jet-overlap region near the center point. Indeed, in the overlap region the two velocity abscissas have values $\mathbf{U}_1 = [0\ 1]^T$ and $\mathbf{U}_2 = [-1\ 0]^T$, which correspond to the average velocity boundary condition on the lower and right-side walls, respectively.

### 4.2.2. Particle-wall rebound

In the next example, we consider a particle jet rebounding off a reflective wall. In this flow, the particle jet enters through the left-hand side of the domain with average velocity $\mathbf{U}_p = [1\ \ -1]^T$ (see Fig. 4). The jet

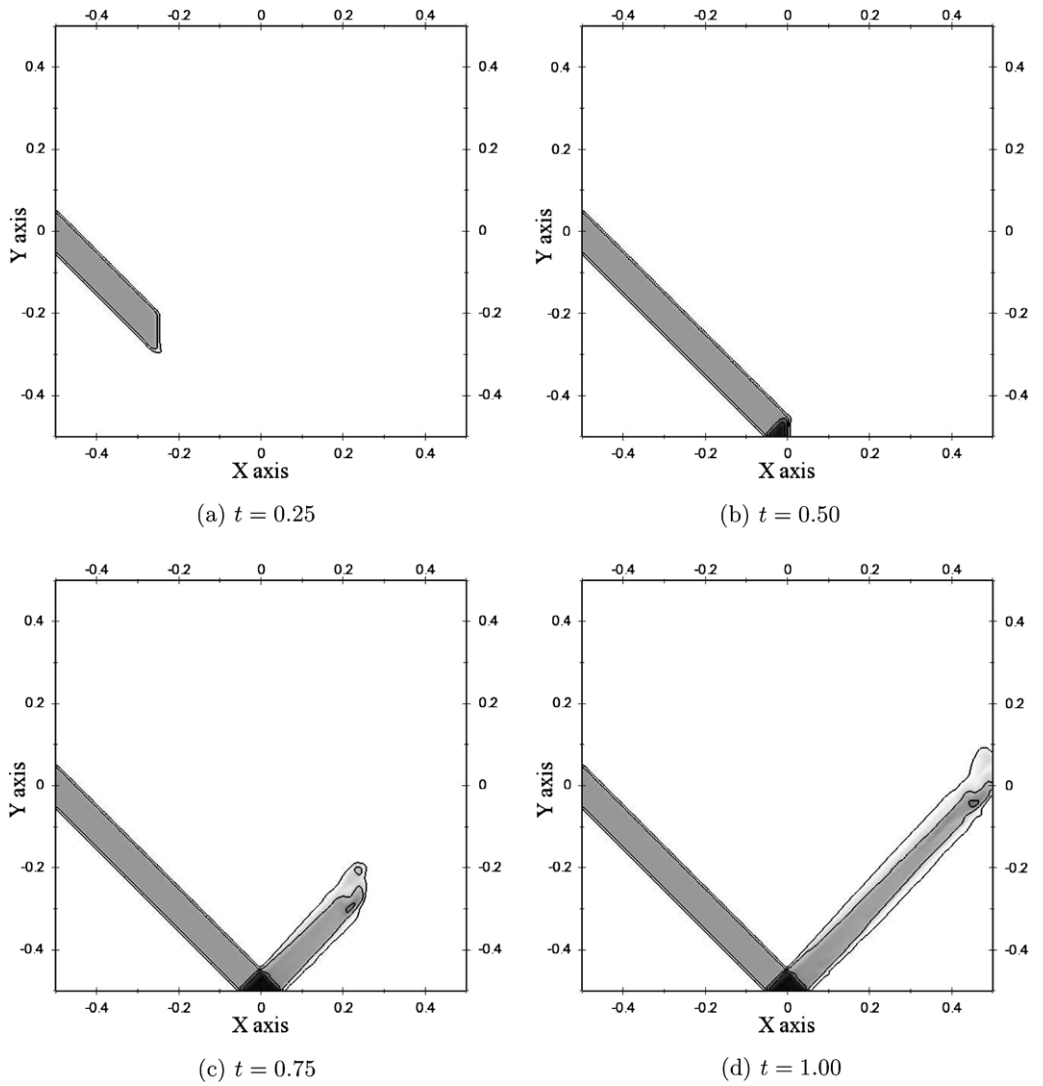


Fig. 4. Time evolution of particle number density for particle-wall rebound.

proceeds towards the bottom wall where it is reflected back into the box before exiting from the left-hand side. The boundary condition along the bottom wall is straightforward to implement in terms of the velocity abscissas. We simply change the $y$ component of the node velocities as follows: $\mathbf{U}_{n2} \rightarrow -e\mathbf{U}_{n2}$ where $e = 1$ is the coefficient of restitution, and adjust the weights to conserve mass. Thus, one can easily simulation particle rebounds off of partially reflective walls by choosing $0 < e < 1$. Note that in this example, the particle velocity is bivariate near the impingement point at the wall due to the incoming velocity of $[1 \ -1]^{\mathrm{T}}$ and the outgoing velocity of $[1 \ e]^{\mathrm{T}}$. Thus, the average velocity just above the wall is $[1 \ (e-1)/2]^{\mathrm{T}}$. Because most moment closures use the average velocity for convective transport, they are not able to reflect particles from the wall. Once again, the two-node quadrature closure overcomes this difficulty in an intuitive and straightforward manner.

These three examples without fluid coupling clearly demonstrate the power of quadrature-based moment closures to represent the dynamics of non-equilibrium particle flows. In the next set of examples, we add fluid coupling and compare the Eulerian moment closure directly to Lagrangian simulations for the same flows. In each example, we will assume that the fluid velocity field is known and unaffected by the particles. We will then initialize a particle field with a given Stokes number in a region of the flow, and allow it to evolve through the combined effects of transport and drag. The Eulerian description will be based on the two-node closure. The Lagrangian description will use a large ensemble of particles initialized in such a way to be exactly consistent with the moments used in the Eulerian model. Although it would in principle be possible to compare predictions for any of the moments used in the Eulerian description, we will concentrate on comparisons at the level of the particle number density, which can be estimated from Lagrangian simulations with an acceptable level of statistical error.

#### 4.2.3. Taylor–Green flow

In the first set of examples with fluid coupling, we will assume that the fluid is described by Taylor–Green (TG) flow in a periodic domain [4,26] (see Fig. 5). The particle field is initialized such that all particles are uniformly distributed in a small circle just above the center of a TG vortex, and the initial particle velocity is the same as the fluid velocity at the same location. Locating the particles off center breaks the symmetry of the particle flow, and thus makes the effect of the particle Stokes number easier to observe. For zero Stokes, the particles velocity is exactly equal to the fluid velocity, and the circle of particles simply rotates about the center point without changing shape. For finite but small Stokes, the particle behavior depends on a critical Stokes number $St_c = 1/(8\pi) \approx 0.04$ [23,24]. Below $St_c$, the particles will remain inside of a TG cell for all times without particle-crossing trajectories, eventually approaching the four corners of the TG cell where the fluid velocity is null. Above $St_c$, at least some of the particles will escape their original TG cell and enter neighboring cells. In general this will lead to particle-crossing trajectories, with the number increasing with

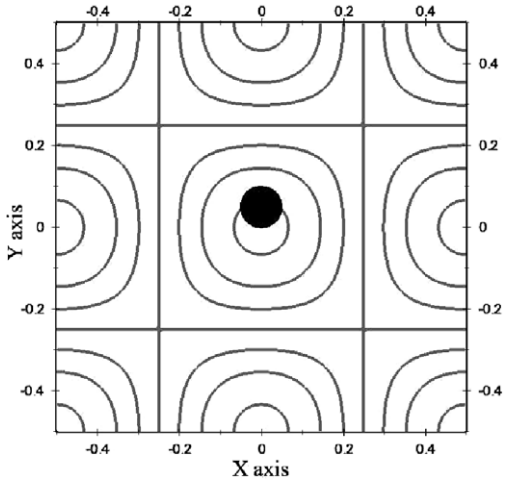


Fig. 5. Initial conditions used for Taylor–Green flow examples. Solid circle represents the particle locations and the curves represent fluid streamlines.

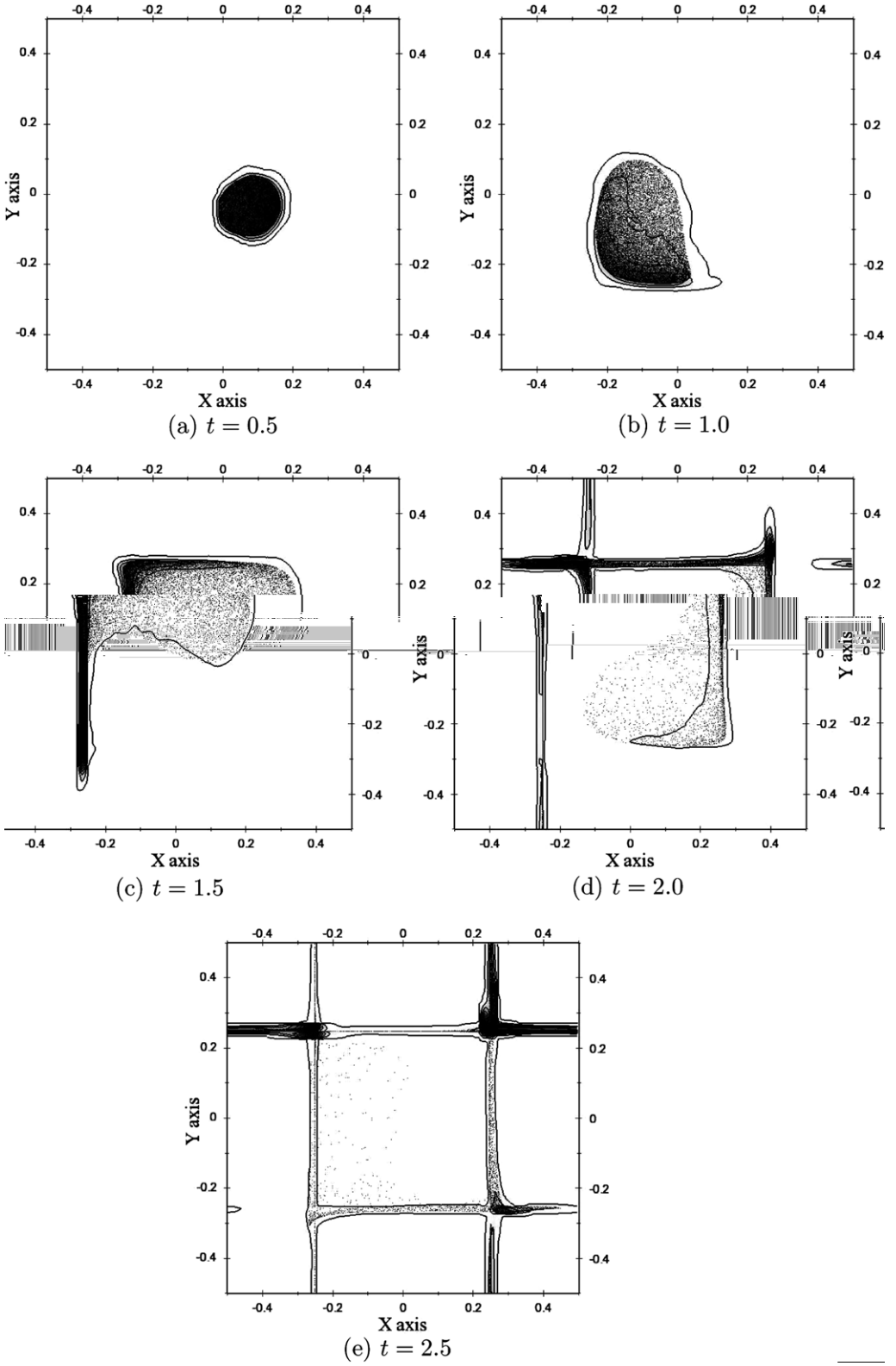


Fig. 6. Time evolution of particle number density in Taylor–Green flow for $St = 0.1$. Contours: 10 levels uniformly spaced between 0 and 5.

increasing Stokes number. For Stokes number below $St_c$, the Eulerian model based on the one-node quadrature closure is in excellent agreement with the Lagrangian simulations [4]. We will thus consider only examples where the one-node closure breaks down above $St_c$.

In the first example, the Stokes number is set to 0.1. Contour plots found from the two-node closures overlaid with the Lagrangian particle positions are shown in Fig. 6. For this Stokes number, particle-crossing trajectories occur only near the corners of the TG cells. However, it can clearly be observed that by $t = 1.5$ particles have begun to leave their original TG cell and are accumulating along the cell walls. Due to the periodic nature of the flow domain, particles that leave from the left/bottom (see $t = 2.0$) are returned at the right/top. Although difficult to assess in a quantitative manner due to the relatively high concentration of the particles near the walls, it is evident that the agreement between the Lagrangian and Eulerian particle distributions is at a minimum qualitatively good. Finally, we can report that the one-node closure begins to fail for this Stokes number at the time where the particles first begin to leave their original TG cell. Just as in the example in Fig. 2, this breakdown is caused by the inability of the one-node closure to describe the particle-crossing trajectories that occur when particle cross cell boundaries.

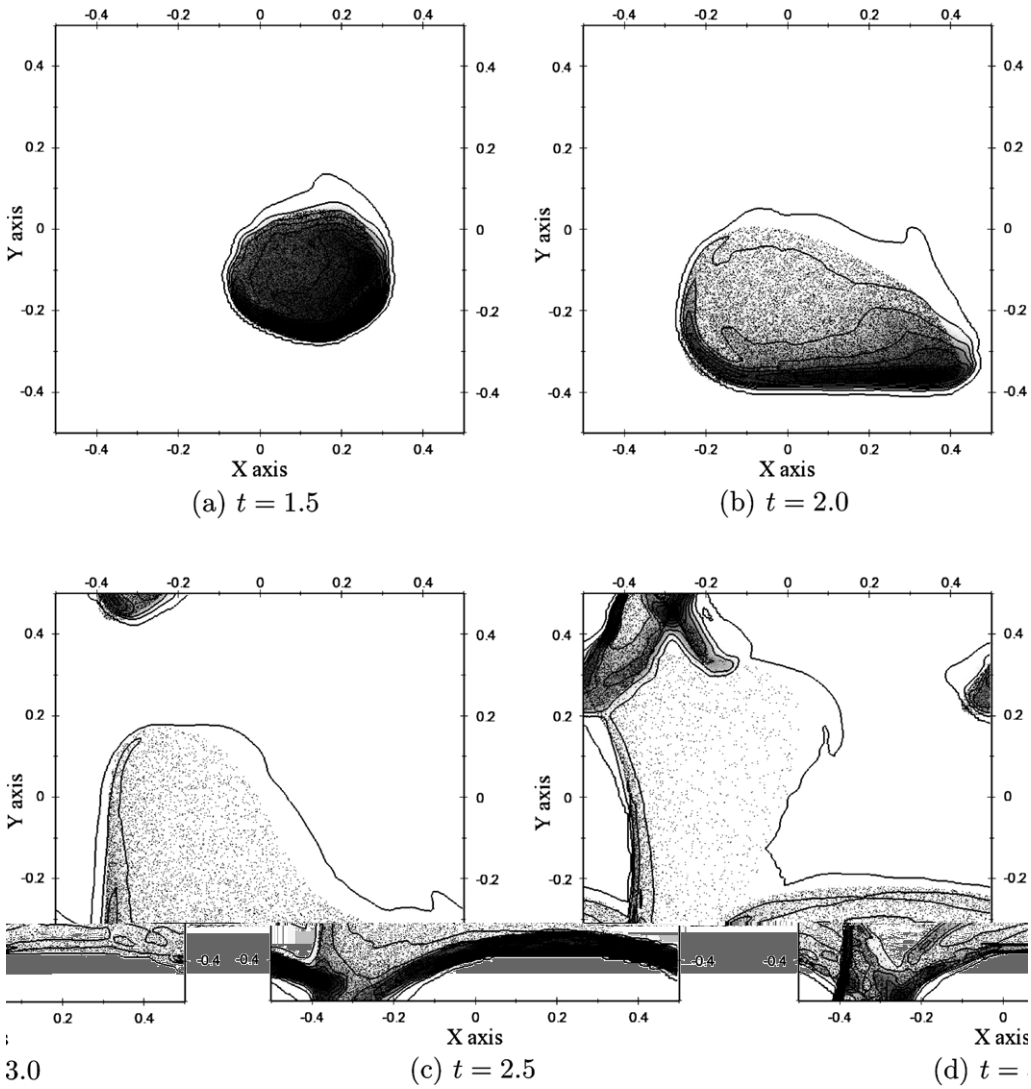


Fig. 7. Time evolution of particle number density in Taylor–Green flow for $St = 1$. Contours: 10 levels uniformly spaced between 0 and 1.2.

In the second example, shown in Fig. 7, the Stokes number is set to 1.0. For this Stokes number, the particles do not respond quickly to the fluid drag and particle-crossing trajectories occur quite often. By $t = 1.5$ the particles start to cross the lower and right boundaries of their original TG cell. By $t = 2.0$ the majority of the particles are in the lower TG cells where the local fluid velocity is directed upward. In other words, the fluid drag is working to decelerate the particles. This results in a local accumulation of particles at $t = 2.5$ and eventually ($t = 3.0$) some of the particles move in the opposite direction. Thus, in this region of the flow the particle velocity distribution is bimodal at each point (i.e., there are particles moving upward and downward at the same point). The two-node closure successfully handles these flow structures without creating "singularities" in the particle number density. Particle-crossing trajectories can be observed at several other locations in the flow (lower left corner at $t = 2.5$, upper left corner at $t = 3.0$). One can also observe that the agreement between the Lagrangian and Eulerian particle distributions is again excellent.

Finally, a comparison between the one-node and two-node closure predictions at $t = 3$ is shown in Fig. 8. As is characteristic of all Eulerian models that cannot explicitly represent more than one local particle velocity, the one-node closure exhibits local "delta-shocks" [3,24,4] where particles accumulate whenever particles are traveling in two directions at the same point. Thus, for example, in the one-node closure we do not observe in the lower-right corner particle "clouds" moving upward and downward, as is observed in the Lagrangian simulations and with the two-node closure. Instead, all of the particles concentration on thin "bands" that are convected with the local average particle velocity. Note that the thickness of these bands is entirely dependent on the grid resolution used to solve the problem (i.e., a sort of "numerical" segregation that is unphysical). Thus, the numerical solution of the one-node model will never be grid independent. This behavior is completely analogous to that seen in one spatial dimension (Fig. 2). The overall conclusion is that Eulerian models that cannot represent explicitly multiple local velocities lose accuracy very quickly for particles with finite Stokes number.

In the third example, shown in Fig. 9, the Stokes number is set to 10. For this Stokes number, the particles respond very slowly to the fluid drag and particle-crossing trajectories are ubiquitous in the periodic flow domain. Up to $t = 7$ we can observe that the agreement between the Lagrangian and Eulerian simulations is excellent. However, by $t = 8$ and especially at $t = 10$, significant differences are plainly visible. The reason for the eventual degradation of the prediction from the two-node closure is straightforward. At this Stokes number multiple particle-crossing trajectories (i.e., more than two) will occur as the particles exit and renter the periodic domain at various angles. By definition, the two-node closure can only describe two particle velocities at any point. Thus, when three particle trajectories cross, the two-node closure replaces the three velocities with only two, while preserving the set of $2(1 + d)$ lower-order moments used to define the two-node closure.

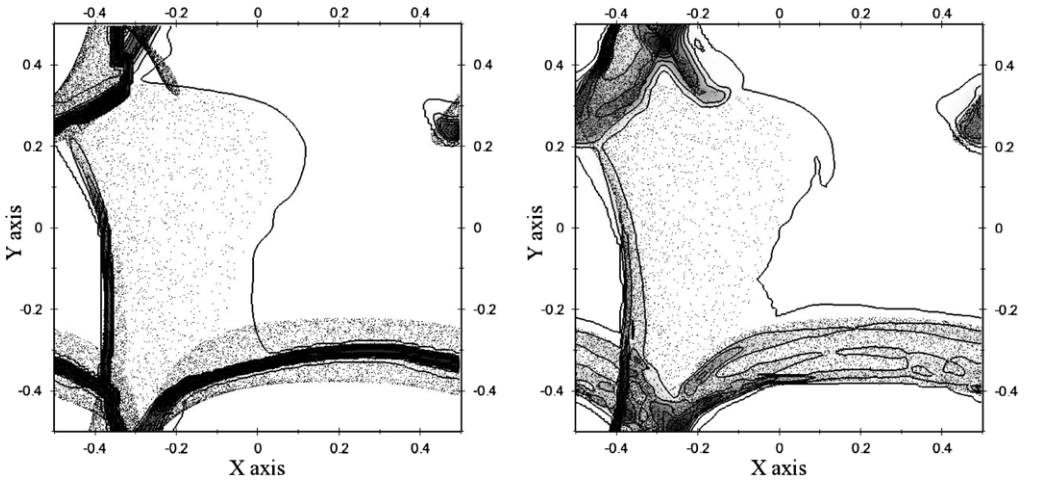


(a) One-node closure (b) Two-node closure

Fig. 8. Comparison of particle number densities in Taylor–Green flow for $St = 1$. Contours: 10 levels uniformly spaced between 0 and 1.2.

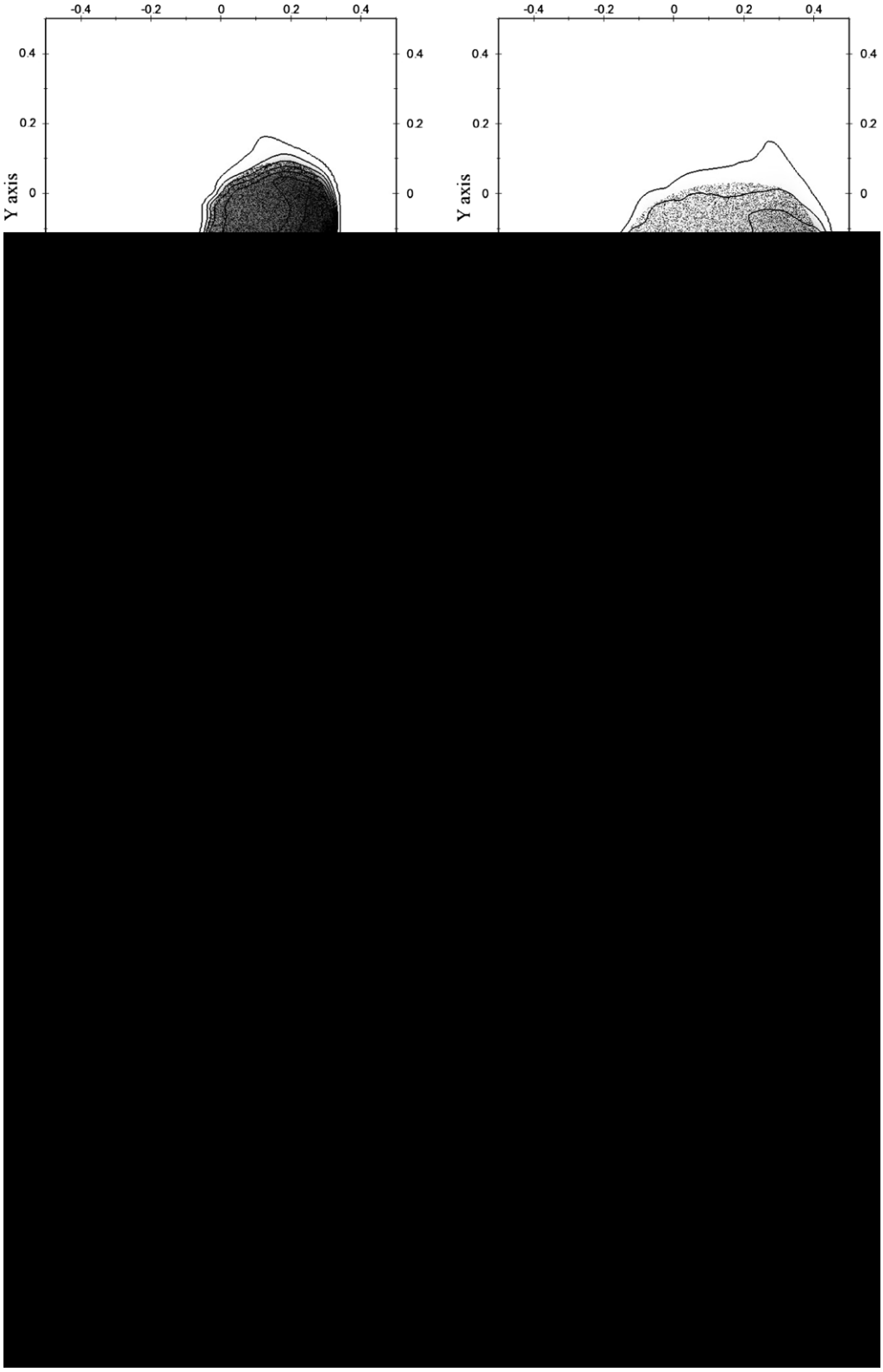


Fig. 9. Time evolution of particle number density in Taylor–Green flow for $St = 10$. Contours: 10 levels uniformly spaced between 0 and 1.2.

In a two-dimensional flow, six moments are required to define uniquely two velocities, but nine would be required to define three velocities. While a quadrature-based moment closure with more than two nodes would allow us to handle multiple particle-crossing trajectories, it is obvious that large Stokes number particles in periodic domains will eventually exhaust all of the available nodes. Nevertheless, it is remarkable that the quadrature-based closure agrees with the Lagrangian simulations for as long as it does for this difficult example. In comparison, other Eulerian models break down much earlier due to their inability to capture particle-crossing trajectories.

### 4.3. Three-dimensional test case

#### 4.3.1. Frozen homogeneous isotropic turbulence

For this test case, we use a "frozen" three-dimensional homogeneous isotropic turbulence field [25,31] with a Taylor-scale Reynolds number of $R_\lambda = 56$ to represent the fluid. A $128^3$ computational grid is employed to solve the quadrature-based closures. The same fluid field is used with $10^7$ particles to estimate the particle number density using Lagrangian particle tracking. A two-dimensional slice from the fluid vorticity field is shown in Fig. 10. The Lagrangian particles are distributed uniformly in the 3D domain at time $t = 0$, and their initial velocities are set to that of the fluid. The corresponding moments of the particle number density function (which are uniform throughout the domain) are used to initialize the Eulerian models. The Stokes number based on the eddy-turnover time ($t_e$) and the particle response time is $St = 0.3$, while that based on the Kolmogorov time scale is $St_\eta = 6.93$.

Example results are shown in Fig. 11. In the first column of this figure, we plot the actual $x$–$y$ particle locations for Lagrangian particles in the same $128 \times 128 \times 1$ slice through the 3D computational domain as was used in Fig. 10. In the second column of Fig. 11, we plot the Lagrangian number density estimated by counting the number of particles in each grid cell. Note that because the total number of particles is greater than the total number of grid cells by only a factor of 4.77, the estimated Lagrangian particle number density is relatively noisy. In the third column of Fig. 11, we plot the number density found using one-node quadrature (i.e., the two-fluid model), while the two-node closure results are shown in the fourth column.

Results for four different times (scaled by $t_e$) are shown in Fig. 11. At $t = 0.5$, we can observe from the Lagrangian results that the particles are beginning to exhibit zones of preferential concentration with finite widths. In contrast, the one-node quadrature results exhibit local delta-shocks where all of the particle number density appears to be concentrated. Note that these delta-shocks do not, in general, appear in

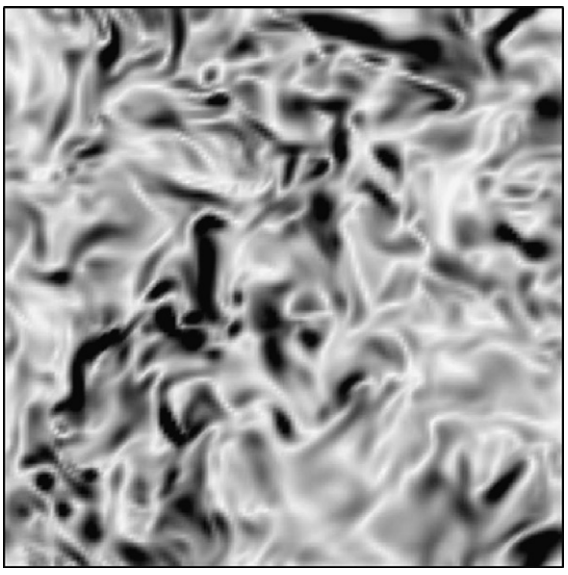

Fig. 10. Frozen fluid vorticity field for homogeneous turbulent flow example with $R_\lambda = 56$. Same $x$–$y$ plane is used in Fig. 11.

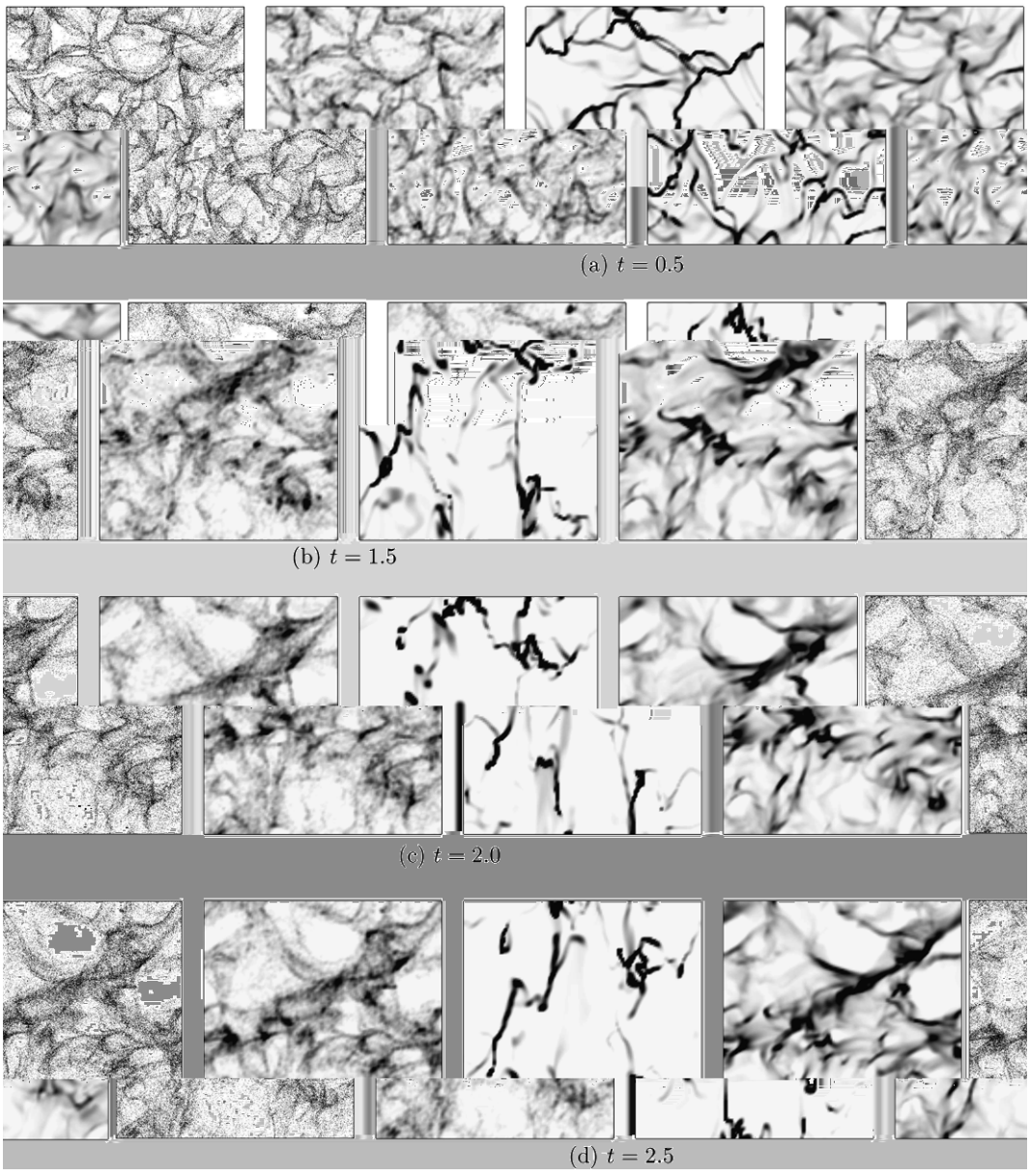


Fig. 11. Evolution of the Lagrangian particle positions and number density in frozen homogeneous turbulent flow for $St = 0.3$. First column: Particle locations. Second column: Lagrangian number density. Third column: One-node quadrature. Fourth column: Two-node quadrature. Color scale for columns 2–4: white is zero and black is equal to five times the volume-averaged number density.

the same locations as the preferential concentration zones. Remarkably, two-node quadrature exhibits preferential concentration zones of finite width and in the same locations as the Lagrangian simulations. Unfortunately, even with $10^7$ Lagrangian particles, the 3D moment fields computed from Lagrangian particle tracking are too noisy to allow for quantitative comparisons with the Eulerian models. This observation is consistent with [4] where $16 \times 10^6$ particles were required in quasi-2D simulations to obtain reasonably converged statistics.

Because the fluid velocity field is stationary, one would expect the Eulerian solver to approach a steady-state solution. Likewise, the Lagrangian solver will approach a dynamic steady state where the particles continue to move, but the statistics approach steady-state values (with time-dependent fluctuations due to the

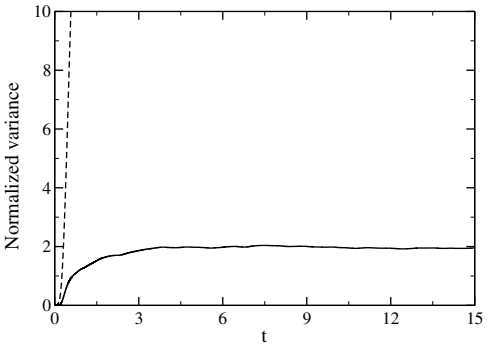


Fig. 12. Normalized volume-averaged variance of the number density computed from the Eulerian models in frozen homogeneous turbulent flow for $St = 0.3$. Dashed: One-node quadrature. Solid: Two-node quadrature.

finite number of Lagrangian particles). As seen in Fig. 11, the results at $t = 2$ are close to the steady-state values for the Lagrangian simulation and for two-node quadrature. As observed at earlier times, the zones of preferential concentration are again coincident for the Lagrangian simulation and two-node quadrature. The same is true at $t = 2.5$, where the two-node closure results appear to have reached a steady state. In contrast, the one-node closure never reaches steady state. Instead, the number density field is made up of time-dependent (and grid-dependent) delta-shocks whose location and evolution is highly sensitive to the numerics. The difference between the two Eulerian models is illustrated in Fig. 12 where we compare the normalized volume-averaged variance of the number density found from both closures. It can be seen that the one-node closure quickly generates a very large variance because of the formation of delta-shocks. In contrast, the variance for two-node closure reaches a steady-state value near two for $t > 3$. It is remarkable that the number density predicted by the two-node closure at $t = 2.5$ in Fig. 11 has a structure that closely resembles that of the Lagrangian simulation, while for the one-node closure it is completely different (e.g. zones of high number density are predicted where the Lagrangian simulation has no particles).

## 5. Conclusions

A two-node quadrature-based moment closure for the Williams spray equation has been derived and verified for one- and two-dimensional, non-equilibrium, dilute, fluid-particle flows. In contrast to the "standard" Eulerian multi-fluid model, two-node quadrature can successfully handle flows with particle-crossing trajectories and thus is able to compute accurately the lower-order velocity moments previously obtainable only by employing a Lagrangian method. While further work is needed to extend the quadrature method to higher order (e.g. three-node quadrature), the ability to compute accurate particle velocity statistics (including, for example, particle energy spectra) in an Eulerian framework should make the quadrature-based models very attractive for many applications involving dispersed-phase flows. Moreover, because quadrature methods are well suited from approximating collision/coalescence terms, it should be relatively straightforward to include such effects in the Eulerian model developed in this work. Finally, because kinetic equations are employed in many fields of physics, the quadrature-based moment closure should find use in many other applications (such as the simulation of rarefied gas flows far from equilibrium [2], and microbubble-laden flows [12]) that are currently treated using Lagrangian methods.

## Acknowledgements

R.O.F. wishes to thank Prof. Marc Massot of the Ecole Centrale, Paris, for first suggesting that quadrature methods might be useful for treating non-monokinetic flows. This work was initiated at the Center for Turbulence Research, Stanford University, during the 2006 Summer Program. The authors gratefully acknowledge financial support from CTR. R.O.F. acknowledges support from US National Science Foundation (CTS-0403864) and the US Department of Energy.

## References


[1] A.E. Beylich, Solving the kinetic equation for all Knudsen numbers, Physics of Fluids 12 (2000) 444–465.
[2] G.A. Bird, Molecular Gas Dynamics and the Direct Simulation of Gas Flows, vol. 42, Oxford Science Publications, 1994.
[3] F. Bouchut, On zero pressure gas dynamics, Advances in Kinetic Theory and Computing. Series on Advances in Mathematics for Applied Sciences 22 (1994) 171–190.
[4] S. de Chaisemartin, F. Laurent, M. Massot, J. Réveillon, Evaluation of Eulerian multi-fluid versus Lagrangian methods for the ejection of polydisperse evaporating sprays by vortices, Journal of Computational Physics, submitted for puiblication. Available from: <http://hal.archives-ouvertes.fr/hal-00169721/fr/>.
[5] P. Colella, A direct Eulerian MUSCL scheme for gas dynamics, SIAM Journal of Scientific and Statistical Computing 6 (1) (1985) 104–117.
[6] J.K. Dukowicz, A particle-fluid numerical model for liquid sprays, Journal of Computational Physics 35 (2) (1980) 229–253.
[7] S. Deshpande, A second order accurate, kinetic theory based, method for inviscid compressible flows, Techical Report, NASA Langley, vol. 2613, 1986.
[8] O. Desjardins, R.O. Fox, P. Villedieu, A quadrature-based moment closure for the Williams spray equation, in: Proceedings of the Summer Program 2006, Center for Turbulence Research, Stanford, 2006, pp. 223–234.
[9] G. Dufour, P. Villedieu, A second-order multi-fluid model for evaporating sprays, Mathematical Modelling and Numerical Analysis 39 (5) (2005) 931–963.
[10] J.L. Estivalezes, P. Villedieu, High order positivity preserving schemes for the compressible Euler equations, SIAM Journal of Numerical Analysis 33 (5) (1996) 2050–2067.
[11] A. Ferrante, S. Elghobashi, On the effects of microbubbles on the Taylor–Green vortex flow, Journal of Fluid Mechanics 572 (2007) 145–177.
[12] A. Ferrante, S. Elghobashi, On the accuracy of the two-fluid formulation in direct numerical simulation of bubble-laden turbulent boundary layers, Physics of Fluids 19 (4) (2007) 045105.
[13] R.O. Fox, Computational Models for Turbulent Reacting Flows, Cambridge University Press, Cambridge, 2003.
[14] R.O. Fox, F. Laurent, M. Massot, Numerical simulation of spray coalescence in an Eulerian framework: direct quadrature method of moments and multi-fluid method, Journal of Computational Physics, in press, doi:10.1016/j.jcp.2007.10.028.
[15] A. Kaufmann, M. Moreau, O. Simonin, J. Helie, Comparison between Lagrangian and mesoscopic Eulerian modelling approaches for inertial particles suspended in decaying isotropic turbulence, Journal of Computational Physics, submitted for publication.
[16] A. Kaufmann, O. Simonin, T. Poinsot, Direct numerical simulation of particle-laden homogeneous isotropic turbulent flows using a two-fluid model formulation, in: Proceedings of Fifth International Conference on Multiphase Flow (ICMF'04), 2004.
[17] F. Laurent, M. Massot, Multi-fluid modeling of laminar poly-dispersed spray flames: origin, assumptions and comparison of the sectional and sampling methods, Combustion Theory and Modelling 5 (2001) 537–572.
[18] F. Laurent, M. Massot, P. Villedieu, Eulerian multi-fluid modeling for the numerical simulation of polydisperse dense liquid spray, Journal of Computational Physics 194 (2004) 505–543.
[19] R. Leveque, Finite Volume Methods for Hyperbolic Problems, Cambridge University Press, Cambridge, 2002.
[20] D.L. Marchisio, R.O. Fox, Solution of population balance equations using the direct quadrature method of moments, Journal of Aerosol Science 36 (2005) 43–73.
[21] D.L. Marchisio, J.T. Pikturna, R.O. Fox, R.D. Vigil, A.A. Barresi, Quadrature method of moments for population balances with nucleation, growth and aggregation, AIChE Journal 49 (2003) 1266–1276.
[22] D.L. Marchisio, R.D. Vigil, R.O. Fox, Quadrature method of moments for aggregation-breakage processes, Journal of Colloid and Interface Science 258 (2) (2003) 322–334.
[23] M. Massot, Personal communication.
[24] M. Massot, Eulerian multi-fluid models for polydisperse evaporating sprays, in: D.L. Marchisio, R.O. Fox (Eds.), Multiphase Reacting Flows: Modelling and Simulation, CISM Courses and Lectures, vol. 492, Springer, Vienna, 2007, pp. 79–123.
[25] M. Massot, C. Knikker, C. Péra, J. Réveillon, Lagrangian/Eulerian analysis of the dispersion of evaporating sprays in non-homogeneous turbulent flows, in: Proceedings of Fifth International Conference on Multiphase Flow (ICMF'04), 2004.
[26] M. Massot, F. Laurent, S. de Chaisemartin, Eulerian multi-fluid method for the numerical simulation of evaporating polydisperse sprays: modelling and numerical issues in multi-dimensional configurations, in: Proceedings of Sixth International Conference on Multiphase Flow (ICMF'07), 2007.
[27] R. McGraw, Description of aerosol dynamics by the quadrature method of moments, Aerosol Science and Technology 27 (1997) 255–265.
[28] B. Perthame, Boltzmann type schemes for compressible Euler equations in one and two space dimensions, SIAM Journal of Numerical Analysis 29 (1) (1990) 1–19.
[29] D.I. Pullin, Direct simulation methods for compressible inviscid ideal gas-flows, Journal of Computational Physics 34 (1980) 53–66.
[30] M. Reeks, On a kinetic equation for the transport of particles in turbulent flows, Physics of Fluids A 3 (3) (1991) 446–456.
[31] J. Réveillon, M. Massot, C. Péra, Analysis and modeling of the dispersion of vaporizing polydispersed sprays in turbulent flows, in: Proceedings of the Summer Program 2002, Center for Turbulence Research, Stanford, 2002, pp. 393–404.
[32] L. Sainsaulieu, Equilibrium velocity distribution functions for a kinetic model of two-phase flows, Mathematical Models and Methods in Applied Sciences 5 (2) (1995) 191–211.
[33] L. Schiller, A. Nauman, A drag coefficient correlation, V.D.I. Zeitung 77 (1935) 318–320.

[34] B. van Leer, Towards the ultimate conservative difference scheme. V. A second-order sequel to Godunov's method, Journal of Computational Physics 32 (1979) 101–136.
[35] L. Wang, D.L. Marchisio, R.D. Vigil, R.O. Fox, CFD simulation of aggregation and breakage processes in laminar Taylor–Couette flow, Journal of Colloid and Interface Science 282 (2005) 380–396.
[36] F.A. Williams, Spray combustion and atomization, Physics of Fluids 1 (1958) 541–545.
[37] L.I. Zaichik, An equation for the particle velocity probability density function in inhomogeneous turbulent flow, Fluid Dynamics 32 (2) (1996) 261–267.
[38] A. Zucca, D.L. Marchisio, A.A. Barresi, R.O. Fox, Implementation of the population balance equation in CFD codes for modelling soot formation in turbulent flames, Chemical Engineering Science 61 (2006) 87–95.